Scilight

Materials for the Environment

https://www.sciltp.com/journals/mfe



Review

Dynamic Active-Site Engineering in MOF-Based and MOF-Derived Materials for H_2S Capture and Conversion: From Molecular Adsorption to Mechanisms, Regeneration, and Future Design Principles

Riying Qi, Xufeng Nian, Yuechao Yang, Shirin Jazbia and Qiyong Xu *

Shenzhen Engineering Laboratory for Eco-Efficient Recycled Materials, School of Environment and Energy, Peking University Shenzhen Graduate School, University Town, Xili, Nanshan District, Shenzhen 518055, China

* Correspondence: qiyongxu@pkusz.edu.cn

How To Cite: Qi, R.; Nian, X.; Yang, Y.; et al. Dynamic Active-Site Engineering in MOF-Based and MOF-Derived Materials for H_2S Capture and Conversion: From Molecular Adsorption to Mechanisms, Regeneration, and Future Design Principles. *Materials for the Environment* **2026**, *1*(1), 4.

Received: 31 July 2026
Revised: 10 September 2026
Accepted: 16 September 2026
Published: 29 September 2026

Abstract: Hydrogen sulfide (H_2S) removal is important for protecting energy conversion systems, reducing environmental emissions. Metal-organic frameworks (MOFs) are promising materials for H_2S removal because they have tunable pore structures, coordination environments, and adjustable chemical functionalities. However, most studies have evaluated these materials based on adsorption capacity and static structural properties. Changes in active sites during H_2S adsorption, sulfur speciation, deactivation, and regeneration are still not well understood. This review presents a dynamic active site engineering perspective on MOF-based adsorbents during the H_2S removal cycle. MOF-based H_2S adsorbents, including pristine MOFs, functionalized frameworks, MOF-derived carbons, and hybrid materials, are discussed based on their structural characteristics and adsorption behavior. The roles of hierarchical porosity, metal centers, nitrogen functionalities, and metal-support interactions in molecular adsorption, sulfur conversion, and interfacial reconstruction are also discussed. The changes in active sites during H_2S activation, sulfur accumulation, and regeneration are then examined, together with thermal, chemical, and photo-assisted regeneration methods. Finally, advances in operando characterization, theoretical modeling, and artificial intelligence-assisted materials discovery are discussed as tools for linking material structure, active site changes, and H2S removal performance.

Keywords: metal-organic frameworks; hydrogen sulfide removal; dynamic active-site engineering; sulfur conversion; adsorption-regeneration

1. Introduction

Hydrogen sulfide is a toxic and corrosive gas contaminant commonly found in industrial gas streams, including biogas, natural gas, coke oven gas, landfill gas, and refinery off-gases [1–8]. Exposure to H_2S can threaten occupational safety and accelerate equipment degradation through sulfide corrosion and catalyst poisoning [9–13]. Incompletely removed H_2S also forms sulfur oxides during combustion, which can cause acid deposition and secondary particulate pollution [14–16]. As sulfur emission regulations become stricter and renewable gaseous fuels are used more widely, efficient H_2S removal has become an important step in gas purification and catalyst protection [17,18].

Industrial H_2S removal technologies mainly include wet scrubbing, biological desulfurization, membrane separation, catalytic oxidation, and adsorption [19–21]. Wet chemical processes can achieve high sulfur removal

Copyright: © 2026 by the authors. This is an open access article under the terms and conditions of the Creative Commons Attribution (CC BY) license (https://creativecommons.org/licenses/by/4.0/).
Publisher's Note: Scilight stays neutral with regard to jurisdictional claims in published maps and institutional affiliations.

efficiencies, but they usually require large amounts of chemical reagents, produce secondary wastewater, and have high operating costs [20,22]. Biological methods are more environmentally friendly, but they are limited by slow reaction rates and narrow operating conditions [9,23]. Membrane separation allows continuous operation, but it often has limited selectivity and can suffer from membrane fouling when treating sulfur-containing gas mixtures [24–26]. Catalytic oxidation can convert H_2S rapidly, but it usually requires a controlled oxygen supply and a suitable operating temperature. Sulfur accumulation and strongly bound sulfur species can also cause catalyst deactivation over time [9,27,28].

For solid-based H_2S removal, the dominant pathway may range from molecular adsorption and reactive chemisorption to adsorption-coupled catalytic oxidation, depending on the active site chemistry and reaction atmosphere [17,29,30]: (i) molecular adsorption or coordination adsorption. In this mode, the H_2S molecule interacts with the open metal sites or the pore surface through weak coordination bonds or van der Waals forces, without breaking the S–H bond. This process is often reversible under mild conditions; (ii) reactive adsorption or metal sulfidation. During this process, H_2S undergoes dissociative chemical adsorption, forming strong metal-sulfur bonds (such as Cu-S, Zn-S). Because a chemical bond must be broken for the site to be restored, this pathway is usually difficult to reverse and frequently leads to irreversible sulfidation; (iii) adsorption-assisted selective oxidation. The MOF material first captures H_2S through coordination, and then uses lattice oxygen or sites with redox activity (such as Fe^{3+}/Fe^{2+}, Cu^{2+}/Cu^{+}) to selectively oxidize the HS^* or S^* species, generating elemental sulfur. The regeneration process requires re-oxidation and reduction of the metal sites with O_2. MOFs with redox-active linkers or doped with heteroatoms (N, S) belong to this category; (iv) continuous feed catalytic conversion. In this mode, the metal-organic framework functions as a true catalyst rather than an adsorbent. Hydrogen sulfide is supplied together with the continuously supplied oxidant (such as O_2, air) or reactant, and through mechanisms similar to the Claus process or photocatalytic/electrocatalytic oxidation, a continuous conversion to elemental sulfur and H_2O is achieved. The active sites are dynamically regenerated during the reaction process, and the stability of the material under continuous operation conditions is the main evaluation criterion. These pathways should be distinguished because they involve different sulfur products, regeneration behaviors, and performance metrics. Nevertheless, adsorption-based processes can often operate under comparatively mild conditions, accommodate variable gas compositions, and be readily integrated into fixed-bed systems.

The performance of adsorption processes mainly depends on the adsorbent. Conventional materials, including activated carbon, zeolites, metal oxides, and impregnated porous supports, have been widely studied over the past decades [29]. Activated carbon has a high surface area but often relies mainly on physical adsorption unless additional catalytic species are introduced [31]. Metal oxides have a strong chemical affinity toward H_2S, but irreversible sulfide formation often limits regeneration [31,32]. Zeolites have well-defined pore structures but generally show weak sulfur affinity because of their limited variety of active sites [33]. These limitations show that a high surface area alone is not enough for efficient and stable H_2S capture [30]. The adsorption behavior also depends on the chemical identity, spatial distribution, and changes of active sites during sulfur uptake and regeneration [34–36]. MOF-based and MOF-derived materials are therefore promising for H_2S purification because their pore environments and active sites can be adjusted for selective capture, reactive removal, or catalytic sulfur conversion.

MOFs provide another platform for designing adsorbents with adjustable structures. Their crystalline architectures, high porosity, and flexible compositions allow precise control of pore geometry and the coordination environment of metal centers [37]. Both metal nodes and organic linkers can interact with guest molecules. This allows adsorption sites to be designed at the molecular level instead of being added through post-synthetic impregnation [38,39]. By selecting suitable metal ions, organic ligands, and synthetic methods, MOFs can be used to adjust Lewis acidity, electronic structures, defect concentrations, and pore accessibility. This makes MOFs attractive materials for the purification of sulfur-containing gas [38,40–42].

Growing evidence shows that H_2S adsorption in MOFs, especially in frameworks with open or redox-active metal sites, cannot always be explained by conventional adsorption models based only on pore filling or adsorption equilibrium [34,43]. Depending on the framework chemistry and gas composition, sulfur capture may involve multiple elementary processes occurring sequentially or concurrently, including molecular diffusion, coordination with unsaturated metal centers, acid-base interactions, electron transfer, and the formation of metal-sulfur species; in O_2-containing streams, further oxidation to elemental sulfur or oxidized sulfur species may also occur [1,35,44]. For instance, coordinatively unsaturated metal sites may undergo changes in their coordination environment and in redox-active systems, oxidation state, while linker functional groups, structural defects, and adsorbed water may influence H_2S dissociation, proton transfer, and the local hydrogen-bonding environment, particularly under humid conditions [1,44–46]. These changes are not necessarily reversible. Weak coordination interactions and certain redox processes may be reversed during regeneration, whereas metal sulfidation, ligand displacement, sulfur deposition, and framework collapse can result in permanent losses of porosity and active sites [35,43,44].

Accordingly, this review distinguishes reversible changes in active site chemistry from irreversible structural degradation and examines how both affect H_2S uptake, sulfur speciation, regeneration, and cyclic stability.

Recent developments have expanded the design of MOF-based H_2S adsorbents beyond pristine crystalline frameworks [43]. Defect engineering, mixed-metal frameworks, linker functionalization, heteroatom incorporation, and hierarchical pore construction have been used to improve sulfur affinity [41,45,47]. MOF-derived porous carbons and metal/carbon composites produced by controlled pyrolysis have also attracted attention. Thermal transformation can retain some structural features of the parent framework and can also form highly dispersed metal nanoparticles, metal oxides/carbides, and heteroatom-doped carbon matrices, depending on the precursor composition and pyrolysis conditions [30,48]. These derived materials often have higher electrical conductivity and better hydrothermal stability than their parent MOFs [30,49,50]. They can also have high accessible surface area, well-developed pores, adjustable architectures, and well dispersed heteroatoms [48,51].

Although much progress has been made, current knowledge of MOF-based H_2S adsorption is still fragmented. Existing reviews mainly classify materials by composition or synthesis strategy and focus on adsorption capacity and structural properties [1,34,43]. To understand the research landscape of MOF-based materials for H_2S-related applications, a bibliometric analysis was performed using the Web of Science Core Collection database. Publications from 1 January 2006 to 1 July 2026 were retrieved with the search topic "MOFs & hydrogen sulfide". English-language research articles and review papers were included. Duplicate records were identified and removed in two steps using EndNote and VOSviewer to improve data reliability. Bibliometric visualization was performed using VOSviewer (version 1.6.20). Author keywords were analyzed using the full counting method, with the minimum occurrence threshold of five. Synonymous terms, such as "H_2S" and "hydrogen sulfide" were merged, and 242 high-frequency keywords were retained for co-occurrence analysis. In the network, node shows the occurrence frequency of each keyword, line thickness shows the strength of keyword co-occurrence, and different colors show different research clusters. As shown in Figure 1, the keyword co-occurrence network provides an overview of the broader research field related to H_2S studies in the context of MOFs. This network mainly consists of interrelated keywords related to H_2S adsorption, capture, removal, separation, and desulfurization, highlighting the core role of MOFs in H_2S purification. Keywords such as oxidation, catalyst, oxide, and hydrogen peroxide further indicate the increasing interest in H_2S catalytic conversion. Other clusters involving gas sensing, fluorescence, electrocatalysis, and photocatalysis are located at the periphery of the network, reflecting the broader multi-functional applications of MOFs in H_2S-related research rather than the main focus of this review. The H_2S removal domain covered in this review has seen previous studies mainly focusing on adsorption capacity, selectivity, and material design, while the evolution of active sites during H_2S adsorption, sulfur transformation, and regeneration processes has received relatively less systematic attention.

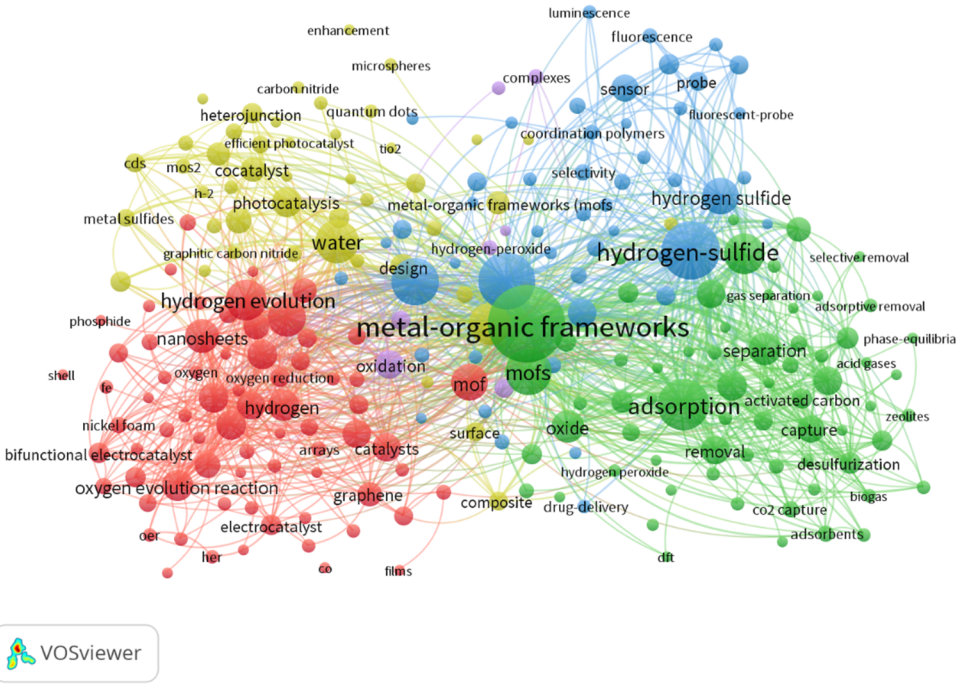


Figure 1. Keyword co-occurrence network of publications on MOF-based materials for H_2S-related applications based on the Web of Science Core Collection database (from 1 January 2006 to 1 July 2026), generated using VOSviewer (minimum keyword occurrence = 5).

This review addresses these issues by studying how to remove H_2S from the perspective of dynamic active site engineering (Figures 2 and 3). Here, "dynamic active-site engineering" refers to the intentional regulation of the configuration of the active site, so that it changes during the processes of H_2S adsorption, sulfur conversion, and regeneration, rather than treating the active site as a static structural entity. In this context, "dynamic" encompasses three interrelated processes: (i) changes in the coordination environment of the metal center, including the breaking, formation, and reconfiguration of metal-ligand or metal-sulfur bonds; (ii) the redistribution of interface electronic structure, including the changes in the oxidation state and charge density of the metal during H_2S activation and sulfur conversion, which may be reversible, partially reversible, or irreversible; (iii) in the regeneration process, the reversible or partially reversible reconfiguration of the metal-heteroatom-carbon interface and surface functional groups. These changes determine whether the active site can still be accessed and remains reactive, whether it evolves into a more active configuration, or is blocked or irreversibly deactivated due to sulfur accumulation. Therefore, dynamic active-site engineering shifts the design principle from maximizing the initial number of active sites to controlling their evolution, adaptability, and reversibility during the adsorption-conversion-regeneration cycle.

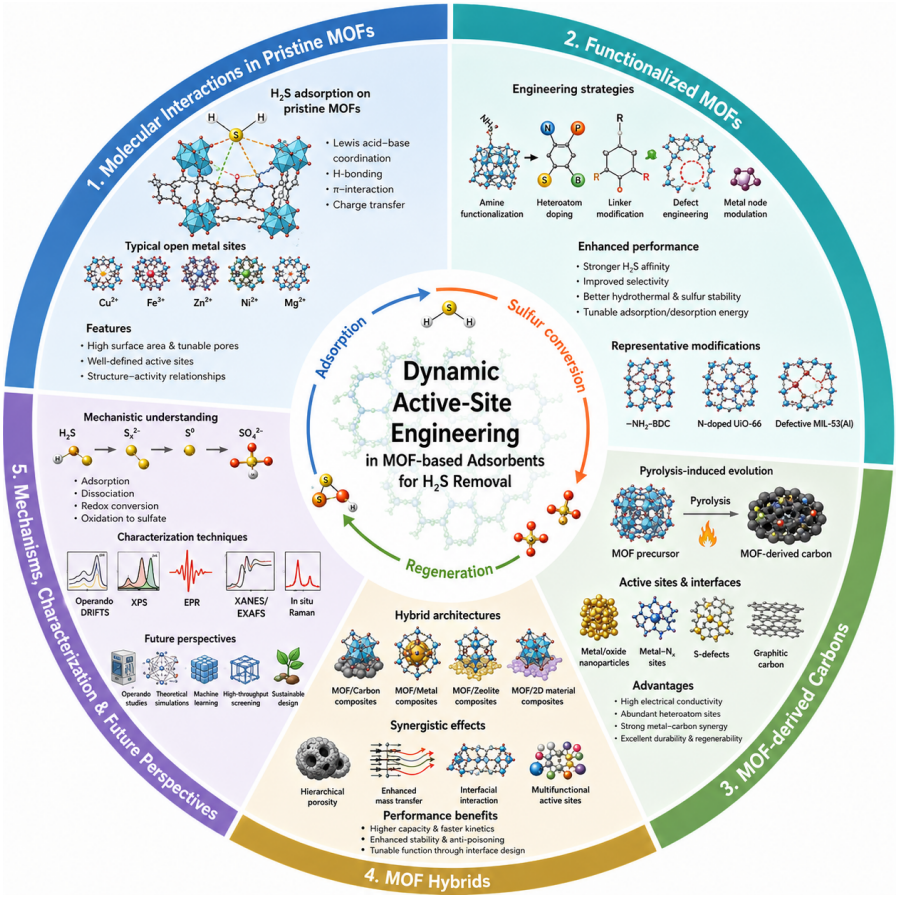


Figure 2. Conceptual diagram providing an overview of the topics covered in this review. The specific engineering strategies, transformation pathways, and active site performances are system-dependent and may vary with material architectures, operating conditions, and atmospheric conditions.

Rather than classifying materials only by framework chemistry, this review focuses on how different active sites change during adsorption, sulfur conversion, and regeneration. The discussion starts with the molecular interactions between H_2S and different adsorption sites in pristine MOFs. It then covers recent advances in the design of metal nodes, organic linkers, and defect structures. Special attention is given to MOF-derived materials, where pyrolysis changes the structure and forms metal-carbon interfaces with coupled catalytic functions. The regeneration of active sites, sulfur-species transformation, and structural stability during repeated operation are then discussed. The second and third sections in this review are organized by material type, as the synthetic pathways determine which types of active sites can be initially obtained; the fourth and fifth sections track the behavior of the active sites in the adsorption-conversion-regeneration cycle. The former focuses on which sites exist in the materials and how their structures are regulated, while the latter explores how these sites behave after the introduction of H_2S. Finally, new opportunities in characterization, theoretical simulations, and machine-

learning-assisted catalyst design are discussed to guide the development of regenerable MOF-based adsorbents for sulfur purification.

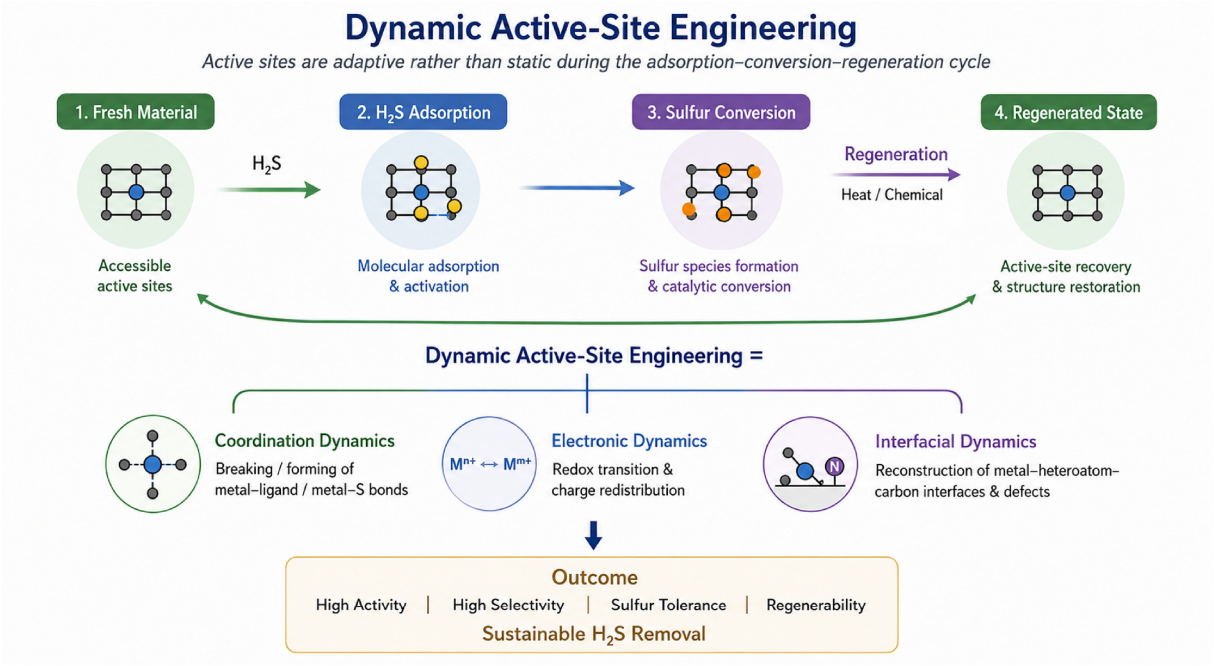


Figure 3. Conceptual diagram illustrating the conceptual framework of dynamic active sites in MOF-based adsorbents for hydrogen sulfide removal. The specific evolution pathways and dynamic behaviors are system-dependent.

2. Major Classes of MOF-Based and MOF-Derived Materials for H_2S Removal

2.1. Pristine MOFs

Pristine metal-organic frameworks are among the first crystalline porous materials studied for H_2S capture because of their adjustable pore structures and chemical environments [43]. Unlike conventional porous adsorbents, such as activated carbons and zeolites, MOFs are formed by coordinating between metal nodes and organic linkers. This structure allows the control of pore size, surface polarity, and adsorption-site chemistry [37].

The H_2S removal performance of pristine MOFs is mainly determined by the type of metal nodes and the accessibility of metal centers rather than surface area alone [1,43]. MOFs with coordinatively unsaturated metal sites (CUSs), including Cu-, Fe-, Ni-, Zn-, and Mg-based frameworks, generally show stronger H_2S uptake than frameworks lacking open metal sites [43,52], as summarized in Table 1. This enhancement arises largely from reactive capture through metal-sulfur bond formation rather than from stronger reversible adsorption, as evidenced by the low capacity retention of Cu-BTC upon cycling. In comparison, ZIF-8, UiO-66, and MOF-801 (as shown in Figure 4) have fewer accessible metal sites, and their H_2S removal is dominated by physisorption and pore confinement rather than by metal-sulfur bond formation [53].

Table 1. Summary of several reported pristine MOF materials for H_2S adsorption (N_2/He balance, standard atmospheric pressure).

MOFs	Cu-BTC	Fe-BTC	Ni-MOF-74	Mg-MOF-74	Zn-MOF-74
BET surface area (m^2/g)	774	/	1193	1244	920
H_2S uptake (mg/g)	38	11.9	409	8	56
Adsorption conditions	30 °C	30 °C	30 °C	25 °C	25 °C
H_2S concentration (ppm)	430	458	59200	10000	10000
Flow rate (mL/min)	30	100	200	/	/
Adsorbent dose (g)	/	/	0.5	/	/
MOF-H_2S Interactions	Cu-S	Fe-S	Ni-S	Mg-S	Zn-S
Cycle(s)	3	/	/	/	/
Capacity retention (%)	15.69 (Cycle 2) 13.72 (Cycle 3)	/	/	/	/
Reversibility	Irreversible	/	Irreversible	Reversible	Irreversible
Reference	[53]	[54]	[55,56]	[57]	[57]

The chemical environment of organic linkers also affects H_2S adsorption. Functional groups in linkers, such as amino, hydroxyl, and oxygen-containing groups, can change framework polarity and provide additional interaction sites for H_2S molecules [1,41,43,45,58]. Pore topology, pore size distribution, and defect concentration also influence molecular diffusion and adsorption capacity. These studies show that the H_2S adsorption performance of pristine MOFs is determined by the combined effect of metal nodes and organic linkers.

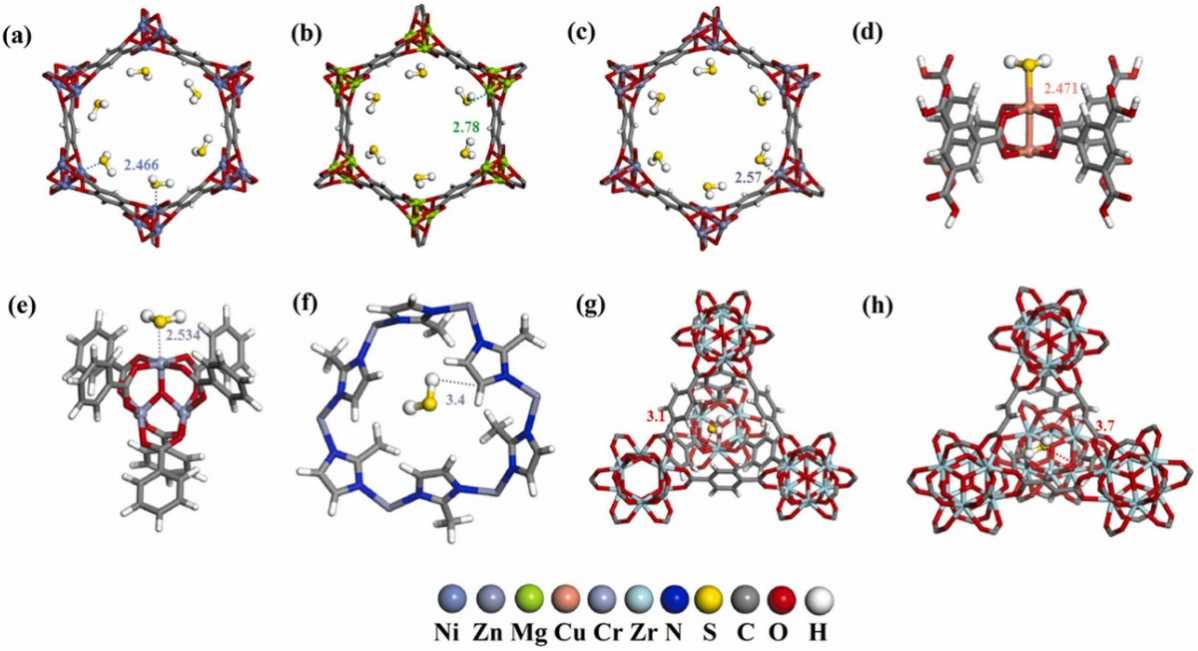


Figure 4. The location of H_2S on MOFs upon adsorption. (**a**) Ni-MOF-74, (**b**) Mg-MOF-74, (**c**) Zn-MOF-74, (**d**) MOF-199, (**e**) MIL-101(Cr), (**f**) ZIF-8, (**g**) UiO-66, (**h**) MOF-801. Reproduced with permission from ref. [53]. Copyright 2023 Elsevier.

The strong interaction between sulfur-containing molecules and metal sites may result in difficult regeneration, and some MOFs show poor chemical stability in humid environments [43]. MOFs with weak metal-ligand bonds may suffer from structural damage during long-term exposure, leading to reduced adsorption capacity and limited recyclability [1,42]. Therefore, although pristine MOFs help reveal the relationship between framework structure and H_2S adsorption, further modifications are needed to improve stability, reversibility and practical applicability.

These limitations have promoted the development of functionalized MOFs, MOF-derived carbon materials, and hybrid structures.

2.2. Functionalized MOFs

Functionalization strategies are mainly used to introduce new adsorption sites and adjust the local chemical environment [43,57]. These modifications can improve H_2S affinity, separation selectivity, and structural stability by regulating surface polarity and electronic properties [42,45]. From the perspective of dynamic active site engineering, functional groups may also influence the behavior of adsorption sites during adsorption and regeneration cycles [38,45].

In the current strategies, amino functionalization has received extensive research because amino groups provide basic sites, which can interact with acidic H_2S through hydrogen bonds and acid-base interactions [1,43]. Although this method is effective, MOFs with amino functional groups usually encounter challenges in large-scale synthesis regarding the cost of ligands and the complexity of the synthesis process. Vaesen et al. [59] demonstrated that functionalizing MIL-125(Ti) with MIL-125(Ti)-NH_2 significantly enhances H_2S/CH_4 selectivity. Despite its excellent performance, large-scale synthesis of MIL-125(Ti)-NH_2 still faces the challenge of incomplete ligand exchange, often resulting in batch-to-batch variability. Grand Canonical Monte Carlo (GCMC) calculations revealed that the grafted amino groups introduce additional hydrogen-bonding interactions with H_2S while maintaining a relatively low adsorption enthalpy, enabling selective adsorption without relying on exposed metal sites.

The amino group is designed as a non-dissociative hydrogen-bonding site, but the same basic site can accept a proton from H_2S to form ammonium hydrosulfide ($NH_4^+SH^-$), converting the captured sulfur into a salt-like

species that is only partially removed by thermal desorption. This pathway drift is consistent with the cycling data in Table 2, where UiO-66-NH_2 retains only 41.8% of its capacity after two cycles, whereas MIL-125(Ti)-NH_2 remains reversible [57]. It should be noted that the uptake values compiled in Table 2 were obtained under different conditions; only within-pair comparisons are meaningful, and the absolute values should not be ranked across studies. Columns 2–5 are within-study pairs, each measured the H_2S removal performance of selected MOFs before and after modification under identical conditions in a single source and therefore directly comparable; the last two columns are from different studies under different conditions and are listed for reference only, not as a before/after comparison. From a scalable synthesis perspective, UiO-66-NH_2 is more amenable to gram-scale production via modulated solvothermal routes; while the high cost of 2-aminoterephthalic acid and the difficulty in removing residual modulators can hinder its industrial-scale fabrication. However, stronger H_2S binding also reduced regeneration efficiency because stable ammonium hydrosulfide species were difficult to remove completely during thermal desorption. Amino functionalization should therefore not be assumed a priori to afford reversible adsorption.

To distinguish reversible active-site evolution from irreversible degradation, this review assesses the reversibility from two perspectives: structure/electronic and function [43,60,61]. Reversibility is assigned from the change trend over multiple cycles rather than from a single end-point comparison: a change is regarded as reversible when both the structural/electronic characteristics (XRD lattice integrity, Brunauer-Emmett-Teller (BET) surface area, metal oxidation state) and the removal performance (capacity, breakthrough time, or sulfur selectivity) recover to a stable plateau, that is, when the loss per additional cycle becomes negligible. When only some structural or functional properties are restored, the change in the active site is classified as partially reversible. Conversely, if the coordination structure continues to be lost, stable metal sulfides or strongly bound sulfur species are formed, the pore structure undergoes irreversible collapse, or performance continues to decline after regeneration, it is regarded as evidence of irreversible degradation. This standard provides a unified basis for comparing the evolution of active sites in different MOF-based adsorption materials.

Table 2. Comparison of the H_2S removal performance of selected MOFs.

MOFs	MIL-125(Ti)	MIL-125(Ti)-NH_2	UiO-66	UiO-66-NH_2	Cu-MOF-199	Cu/NBC
BET surface area (m^2/g)	1179	1245	1322	1097	/	434
H_2S uptake (mg/g)	221	289	8	31	69	158
Adsorption conditions	30 °C	30 °C	25 °C	25 °C	/	25 °C
H_2S concentration (ppm)	/	/	10,000	10,000	/	300
Flow rate (mL/min)	/	/	/	/	50	100
Adsorbent dose (g)	/	/	/	/	/	0.1
Balance gas	CH_4	CH_4	CO_2	CO_2	/	N_2
Pressure (bar)	1	1	1	1	/	/
MOF-H_2S Interactions	H_{OH}-S	H_{OH}-S, H_{H2S}-N_{NH2}, H_{NH2}-S	Aromatic ring-S	NH_2-H_2S Aromatic ring-S	Cu-S	Cu-S
Cycles	/	/	/	2	/	
Capacity retention (%)	/	/	/	41.8	/	
Reversibility	Reversible	Reversible	Reversible	Partially reversible	Irreversible	/
Reference	[43,59]	[43,59]	[57]	[57]	[62]	[30]

Besides amino groups, oxygen-containing functionalities provide another effective route for regulating H_2S adsorption by modifying framework polarity and hydrogen-bonding capability. A systematic comparison of UiO-66(Zr)-X derivatives demonstrated that carboxyl- and hydroxyl-containing substituents produced substantially higher H_2S selectivity than other functional groups because of stronger host-guest interactions [63]. Similar trends were reported for hydroxyl-functionalized MIL-47(V), where hydrogen bonding promoted reversible adsorption [53,64–66]. Sulfonic-functionalized MIL-101(Cr), particularly MIL-101(Cr)-SO_3Ag, further achieved markedly enhanced H_2S uptake together with excellent cyclic stability over five adsorption-desorption cycles [67]. In this case the high uptake originates from reactive sulfidation at Ag^+ sites rather than from polarity regulation, illustrating that the same linker class can support different removal pathways depending on the incorporated cation. These studies suggest that oxygen-containing groups enhance H_2S capture primarily through polarity regulation and specific intermolecular interactions rather than increased surface area.

Halogen functionalization mainly regulates adsorption through electronic effects. Molecular simulations showed that fluorinated and chlorinated MIL-47(V) derivatives maintained high H_2S adsorption capacity and

improved H_2S/CH_4 and H_2S/N_2 selectivity because halogen groups modified the electronic environment of the framework [68–72]. NUM-3a with halogen modification also showed enhanced H_2S adsorption, although its regeneration performance was not reported [73]. Partial fluorination of MIL-101(Cr) further improved H_2S uptake and H_2S/CO_2 selectivity by strengthening interactions between Cr sites and H_2S molecules [74]. However, fluorination could not fully prevent framework degradation after long-term H_2S exposure, indicating that stronger adsorption alone cannot ensure long-term stability [53,67]. Therefore, the effects of halogen functionalization on cyclic stability and regeneration behavior still require further investigation [75,76].

2.3. MOF-Derived Carbons

Although functionalization can improve the adsorption affinity of pristine MOFs, the poor stability of coordination frameworks under sulfur attack, moisture, exposure and structural damage remains a key limitation [42,77,78]. To address these problems, thermal conversion of MOFs into porous carbon materials has been widely studied as an effective approach to construct stable metal-carbon hybrid structures [79–82]. MOF pyrolysis leads to significant structural changes and produces complex interfaces containing carbon framework, dispersed metal species, heteroatom sites, and structural defects [83].

Depending on the metal species, precursor structure, and pyrolysis conditions, different metal-based components, including nanoparticles, metal sites, metal carbides, and metal-N_X sites, can be formed [30,84]. The carbon matrix limits the growth and aggregation of metal species, while the interaction between metals and heteroatoms modifies the electronic properties of active sites. Therefore, MOF-derived carbons can provide adsorption systems that integrate gas enrichment, surface activation, and sulfur conversion, which are difficult to achieve in pristine MOFs.

Cu-based MOF-derived carbon materials are typical examples of this structural transformation. Song et al. [30] reported a Cu-MOF-199-derived N-doped carbon composite (Cu/NBC-600-1), where pyrolysis converted the Cu-BTC framework into a Cu-containing carbon structure. The decomposition of organic ligands formed a porous carbon skeleton, and Cu species were converted into highly dispersed Cu-based nanoparticles confined within the carbon matrix. Unlike pristine MOF-199 with relatively uniform Cu-ligand coordination sites, the derived material contained abundant metal-carbon interfaces and defect-related active regions. These newly formed sites improved resistance to sulfur-induced structural degradation and enhanced the interaction between H_2S molecules and active centers. During the hydrogen sulfide removal process, the porous carbon matrix mainly promotes molecular enrichment and diffusion, while the reconstructed metal-containing interface is conducive to the activation of hydrogen sulfide and further selectively catalyzes its oxidation to elemental sulfur, rather than merely causing chemical adsorption to form stable metal sulfides.

The performance of MOF-derived carbons is closely related to pyrolysis conditions because temperature affects carbon structure, metal dispersion, and interfacial properties [85–87]. Suitable thermal treatment can generate well-dispersed metal species and accessible pore structures. However, excessive carbonization may cause metal particle growth, loss of defects, and reduced accessibility of active sites. Thus, pyrolysis is not only a carbon formation process but also an important method for controlling the distribution and chemical properties of active interfaces.

Their H_2S removal ability is mainly determined by the combined effects of porous carbon structures and reconstructed interfacial sites. Compared with parent MOFs, these materials show better structural stability [88,89].

2.4. MOF Hybrids

The development of MOF-based H_2S adsorbents has gradually changed from improving individual active sites to designing multifunctional interfaces that can combine adsorption, catalytic conversion, and structural stability [43]. MOF-based hybrid materials have been developed by combining MOFs with other functional components. These hybrid structures can overcome the limitations of pristine MOFs and MOF-derived carbons [58].

Based on the incorporated components, MOF hybrids can be divided into three main types: carbon-based composites, metal oxide/MOF heterostructures, and polymer-assisted hybrids. Carbon-supported MOF composites, such as MOF/graphene, MOF/carbon nanotube, and MOF/biochar systems, were first developed to improve the stability and gas transport properties of MOFs. For example, HKUST-1/graphene oxide (GO) composites showed faster H_2S adsorption kinetics than pristine HKUST-1. This improvement was mainly related to better dispersion of MOF particles and the improved accessibility of gas molecules [30,43,77,90–92]. It should be noted that the captured sulfur is not necessarily oxidized to its elemental form in these systems: for HKUST-1/GO composites, reactive adsorption at the unsaturated Cu sites leads to CuS formation, so that retention and sulfidation, rather than selective catalytic oxidation, account for the measured uptake [77]. Notably, this improvement is textural rather than electronic: for HKUST-1/GO composites, and independent electrochemical

measurements on HKUST-1/graphene films showed that graphene incorporation restores conductivity without inducing Cu(II) → Cu(I) reduction. Similarly, UiO-66/GO nanocomposites reached 8.7 mmol S/g at 30 °C, roughly three times the pristine UiO-66, an enhancement ascribed to larger surface area and micropore volume [93]. Interfacial charge transfer is, however, well documented in other MOF-based hybrid systems. More directly relevant to H_2S, the Fe-O-Zr bonds formed in Fe_2O_3@UiO-66 promote electron transfer from Fe to Zr, which suppresses the FeS_2 intermediate that would otherwise be oxidized to SO_2 and thereby raises sulfur selectivity to 93.06% at 150 °C [94]. This establishes that engineering the electron density of the metal center through an interfacial bond is also a viable route to high sulfur selectivity.

MOF/metal oxide hybrid materials represent another important development direction, especially suitable for systems that require both adsorption and catalytic conversion functions. Introducing oxides with redox activity, such as Fe_2O_3 and TiO_2, can overcome the problem of limited reaction activity of traditional MOFs due to their focus on adsorption alone. For instance, Fe_2O_3@UiO-66 exhibits superior sulfur removal performance compared to the parent framework, while the UiO-66/TiO_2 composite still achieves stronger H_2S removal ability despite a reduced surface area [94,95]. Both systems operate through adsorption-assisted selective oxidation: the MOF phase concentrates H_2S, while the redox-active oxide supplies reactive oxygen that converts the sulfur intermediate to elemental sulfur rather than to a metal sulfide. However, excessive oxide loading may lead to pore blockage, reducing the accessibility of MOF adsorption sites, and the accumulation of sulfur during long-term operation remains a challenge [96].

Polymer-assisted MOF hybrid materials are mainly used to improve their moisture resistance and structural durability. The flexible polymer matrix can enhance the stability of the framework under humid conditions and provide additional functional groups for acid gas capture [97,98]. Polyethyleneimine (PEI) functionalization of HKUST-1 grown *in situ* on graphene oxide suppressed the hydrophilicity of the composite and increased the ambient-temperature H_2S uptake from 0.5 to 0.9 mmol S/g per MOF, an 80% improvement, while a HKUST-1/GO hybrid reached 2.1 mmol S/g at 150 °C, 27% above the parent MOF. These effects are structural and chemical rather than electronic. In MOF/conducting-polymer hybrids, coordination between the heteroatoms of polypyrrole and the Zn ions of ZIF-8 has been shown by density functional theory (DFT) to shift the active site and lower the free-energy barrier of the rate-determining step [99], and PEDOT encapsulation raises the conductivity of MIL-101(Cr) to 1.1×10^{-3} S cm^{-1} without sacrificing porosity [100]. The electron-donating or electron-withdrawing character of a coordinated group modulates the electron density at the metal center [101]. It is well established for linker substituents, where -NH_2 and -NO_2 shift the band gap of UiO-66 from 3.64 to 2.76 and 2.92 eV. By analogy, an electron-donating or electron-withdrawing polymer functionality could modulate the electron density at the metal center, influence H_2S dissociation, and facilitate redox cycling and reactive-oxygen generation. However, this possibility has not been verified for a MOF/polymer hybrid under H_2S exposure, for which the available characterization is limited to breakthrough capacity, XRD, FTIR, and porosimetry. It is therefore presented here as a design consideration rather than an established mechanism.

MOF hybrids provide a useful strategy to address the limitations of single-component materials. By combining different components, these materials can achieve improved structural stability, adsorption performance, and catalytic activity.

3. Structure-Function Relationships

The adsorption and catalytic conversion of hydrogen sulfide are related but not exactly the same in terms of structural requirements. In terms of adsorption, the key design goal is to maximize the accessibility and affinity of the hydrogen sulfide binding sites, while avoiding the impact on regeneration performance due to overly strong interactions. Therefore, the pore structure, surface polarity, and Lewis acid-base interactions mainly determine the adsorption capacity and selectivity. In contrast, catalytic conversion requires active sites that can activate H_2S and/or O_2, and promote electron transfer and the conversion of sulfur intermediates. Therefore, for the catalytic conversion of sulfur, metal centers with redox activity, metal-heteroatom interfaces, and structures rich in defects are particularly important. Therefore, an efficient MOF material should balance both functions rather than merely pursuing the maximum adsorption capacity of H_2S.

3.1. Hierarchical Porosity

The adsorption performance of MOF-based materials is closely related to their pore structures, which control molecular transport, active site accessibility, and the interfacial reactions during H_2S removal. Hierarchical porosity provides a suitable structure to regulate gas diffusion, adsorption, and surface reactions at different length scales. The combination of micro-, meso-, and macropores can accelerate H_2S diffusion and allow more gas

molecules to reach active sites before pore blockage or structural damage occurs [102,103]. Therefore, hierarchical pore networks improve active sites utilization and reduce diffusion limitations during repeated adsorption-regeneration processes [104]. Pore structures should be considered as an important part of active site design rather than only a physical property of the material.

Micropores (<2 nm) are the main adsorption regions in most pristine MOFs, because their confined spaces bring H_2S molecules close to coordinatively unsaturated metal sites and facilitate host-guest interactions [103,105]. The short distance between H_2S and metal centers in microporous channels also promotes the formation of metal-sulfur bonds, leading to strong initial chemisorption [55,62]. However, too many micropores may limit gas diffusion, especially during long-term operation. Sulfur intermediates can gradually occupy narrow channels [102]. The accumulation of elemental sulfur or sulfate species can block pore entrances, reduce the accessibility of internal active sites and accelerate performance decay during cyclic adsorption [106].

The incorporation of mesopores (2–50 nm) can reduce these diffusion limitations by providing larger transport channels and more space for sulfur species movement [107]. Mesoporous structures improve the exchange of reactants and products between the gas phase and internal adsorption sites. This effect increases the utilization of active sites located in microporous regions. Faster transport of oxygen, H_2S, and sulfur-containing intermediates helps maintain redox reactions at metal-heteroatom interfaces. It also reduces the accumulation of reaction products that may block catalytic sites [107,108].

While micropores provide the main adsorption capacity, macropores decrease diffusion resistance in packed adsorption beds and improve access to internal pore structures. This advantage becomes more significant at high gas flow rates or high H_2S concentrations [88]. In hierarchical pore materials, macropores act as transport channels, mesopores provide diffusion space, and micropores serve as high-energy adsorption sites [103,108]. The combination of these pore levels creates efficient transport pathways, which help H_2S molecules reach and promote sulfur products removal during regeneration.

Hierarchical porosity also affects the chemical environment around active sites. The formation of mesoporous and defects during framework modification or pyrolysis can expose more coordinatively unsaturated metal sites and generate new interfaces between metal species and heteroatom-doped carbon structures [107,109–111]. For example, theoretical calculation in MOF-derived N-doped carbon systems showed that pyridinic and pyrrolic nitrogen coordinated with Zn provided strong charge transfer and high binding energy for H_2S adsorption [112]. This result indicates that pore structure and active sites are closely connected. In many MOF-derived materials, improved H_2S removal performance is not only caused by larger pore volume but also by the combined effects of pore connectivity, active site exposure, and electronic interactions. For example, hierarchical porous MOF-199 achieved a 34% increase in H_2S breakthrough capacity [102].

Future pore design should focus not only on increasing surface area but also on building hierarchical architectures that balance molecular diffusion and interfacial reaction rates.

3.2. Metal Active Sites

Metal centers are among the most important structural factors controlling H_2S removal in MOF-based adsorbents because they directly afford adsorption affinity, molecular accessibility, and catalytic activity [55,113]. Unlike traditional porous materials, where adsorption mainly depends on surface area and pore volume, MOFs contain well-defined metal coordination structures. The type of metal, coordination environment, and electronic structure of metal centers are key factors determining H_2S removal performance.

Among various structural features, coordinatively unsaturated sites (CUSs) are generally considered the primary adsorption centers for H_2S because exposed metal atoms provide Lewis acidic sites capable of interacting with sulfur-containing molecules [55]. This mechanism is directly evidenced by DFT calculations showing that H_2S preferentially coordinates to the axial position of coordinatively unsaturated sites in M-BTC clusters [114]. MOFs containing open metal sites, such as MOF-74 series, MOF-199, and MIL-101(Cr), usually exhibit stronger H_2S affinity than fully coordinated frameworks because accessible metal centers provide additional binding sites. For example, theoretical calculations have shown that H_2S adsorption on metal centers in MOF-74 and MOF-199 exhibits significantly stronger interaction energies than adsorption on organic linkers, confirming the dominant role of metal sites in sulfur capture [113]. However, the presence of highly accessible metal sites does not necessarily guarantee superior practical performance, because excessively strong metal-sulfur interactions may compromise regeneration efficiency. Table 3 presents the structural-property relationships of several representative MOF materials for the removal of H_2S.

Table 3. Structure-property relationships of representative MOF materials for H_2S removal.

Material	Structural Parameter	Structural Modification	Effect on H_2S Removal	Representative Examples	Ref.
MOF-74	Open metal sites	Exposed Ni/Mg/Co/Cu sites	Enhanced H_2S coordination	Ni-MOF-74	[115]
MIL-100(Fe)	Fe^{2+} CUS density	Thermal activation	Improved O_2 activation and oxidation	MIL-100(Fe)-250	[116]
UiO-66	Defect engineering	Missing-linker defects	Increased accessibility of Zr sites	UiO-66-Fe	[110]
MOF-derived carbon	Metal-carbon interface	Pyrolysis	Adsorption-catalysis coupling	Cu/NBC	[30]
NH_2-MOF	Linker functionality	Amino groups	Stronger H-bond interaction	UiO-66-NH_2	[110,117]

The electronic structure of metal centers further influences the balance between adsorption strength and reversibility. Different metal species exhibit distinct H_2S affinities due to variations in oxidation state, orbital configuration, and coordination environment. Copper-based MOFs have attracted much attention due to their Cu sites having moderate sulfur affinity and good redox flexibility, thereby achieving the dual functions of adsorption and catalytic conversion [60,118]. In contrast, nickel-based frameworks usually have a stronger ability to bind sulfur, but the formation of stable nickel sulfide species can hinder the regeneration process and limit their long-term application in adsorption [119]. Similarly, although Co-based MOFs possess highly accessible Lewis acidic Co^{2+} sites, excessive sulfur affinity may induce framework degradation and irreversible metal sulfide formation, reducing their recyclability [119]. These comparisons indicate that metal selection should consider not only initial H_2S uptake but also the reversibility of metal-sulfur interactions.

The coordination environment around metal centers also affects H_2S adsorption and conversion. For example, ligand substitution or partial linker removal can change the coordination structure of metal atoms and modify their Lewis acidity and adsorption strength. In acetic acid-modulated MIL-53(Fe), the removal of partial linkers exposed more coordinatively unsaturated Fe^{3+} sites and generated additional Lewis acid sites, which improved H_2S removal activity [120]. Defect engineering is another effective method to increase the accessibility of metal sites. Open metal sites generated by defects provide more available positions for H_2S adsorption and reduce steric limitations. For example, benzoic acid-modified MOF-199 produced more unsaturated Cu centers and additional mesopores through defect formation, leading to H_2S uptake [111]. In MIL-100(Fe), the introduction of coordinatively unsaturated Fe sites created a suitable Fe^{2+}/Fe^{3+} redox environment and enhanced H_2S removal performance (Figure 5) [116,120]. However, excessive defect formation may reduce framework stability and accelerate structural degradation under sulfur-containing conditions. Therefore, a proper balance between active site accessibility and structural stability is required.

Multi-metal active sites provide another important strategy for improving sulfur removal performance [121]. Introducing a second metal into the MOF structure can change electronic properties of nearby active centers through electron interaction and charge redistribution. For example, computational studies of bimetallic TM-Cu-BTC systems showed that interaction between Rh-4d/V-3d and S-2p orbitals promoted charge transfer at the interface [122]. Bimetallic MOFs may show different adsorption behavior from single metal systems because of the interaction between two metal centers. For example, Zn-Cu-BTC showed improved H_2S removal after introducing a second metal, which provided additional active sites [121]. In dual-metal MOFs, the two metal species usually play different roles. One metal site can adsorb and activate H_2S, whereas the other metal site can promote sulfur oxidation or assist regeneration through redox reactions [96]. This cooperative effect reduces irreversible sulfur poisoning and improves cycling stability, as demonstrated by hierarchically porous UiO-66-Fe where the synergistic interplay between Fe/Zr bimetallic sites and the hierarchical porous framework strengthens sulfur poisoning resistance while achieving complete H_2S conversion with remarkable stability [110]. These results show that well-designed bimetallic interfaces can improve adsorption capacity, sulfur conversion, and structural stability at the same time [96,110,121].

In MOF-derived carbons and hybrid materials, metal species interact with carbon structures, heteroatoms, or other phases to form multifunctional interfaces. These interfaces provide additional pathways for H_2S adsorption and sulfur conversion. They also improve resistance to sulfur-induced deactivation [30,109,110].

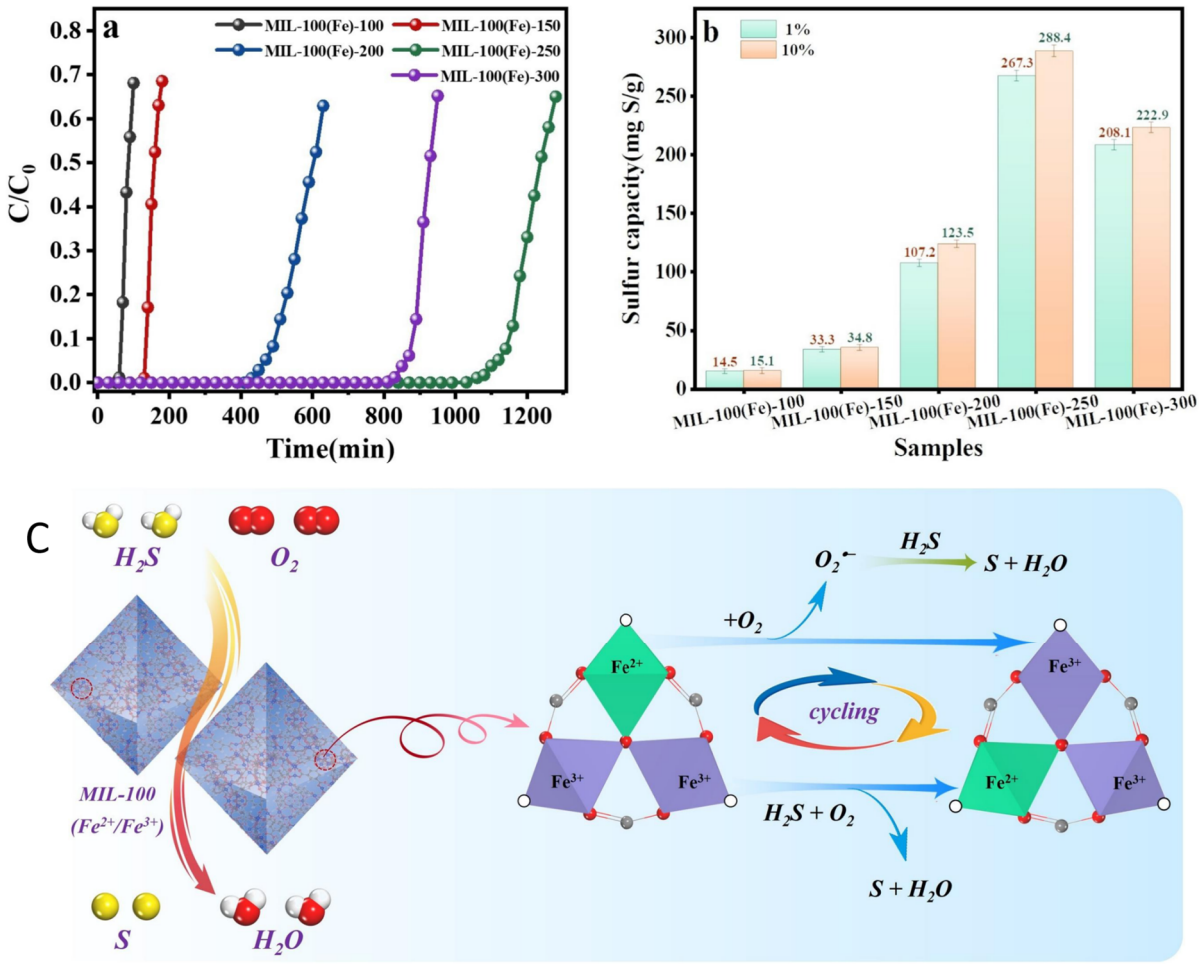


Figure 5. (**a**) The breakthrough curves and (**b**) the breakthrough sulfur capacities of MIL-100(Fe)-T, where T represents the temperature of thermal treatment), (**c**) schematic of H_2S catalytic oxidation over the MIL-100(Fe) catalyst. Reproduced with permission from ref. [116]. Copyright 2025 Elsevier.

Metal active sites provide the main driving force for H_2S adsorption and sulfur conversion. However, their performance depends not only on the initial metal structure but also on the changes in coordination environment and electronic properties during operation. Future metal-site design should not only focus on increasing the number of exposed metal centers but also on controlling their electronic structure, coordination stability, and regeneration ability.

3.3. Nitrogen Functionalities

Nitrogen functionalities are among the most influential structural features in MOF-derived adsorbents because they regulate both the electronic properties of active sites and the physicochemical characteristics of the carbon framework [103,123]. In metal-containing systems, nitrogen species primarily function as electronic mediators that modify charge distribution, stabilize reactive intermediates, and strengthen metal-support interactions. This behavior was directly evidenced by Co-decorated N-doped hollow carbon nanofibers (Co-NHCFs) derived from a bimetallic Zn-Co ZIF, where long-range interactions among Co, N dopants, and the carbon lattice increase the Lewis-basicity of the carbon surface and facilitate H_2S dissociation [123]. In metal-free systems, nitrogen species can directly act as active sites. For example, MOF-derived N-doped mesoporous carbon nanosheets (from ZIF-8) showed high catalytic activity in metal-free H_2S oxidation at room temperature [108]. Nitrogen species do not only improve adsorption capacity but also participate in H_2S activation and sulfur conversion. For example, N-PCNFs (from ZIF-8/PAN) achieved high sulfur capacity because of the combined effects of high nitrogen content and hierarchical porosity [103]. Cu-MOF-derived Cu nanoparticles supported on N-doped biochar also showed efficient H_2S removal capacity through reactive adsorption and catalytic oxidation promoted by the N-doped carbon matrix [30].

Nitrogen atoms in carbon frameworks can exist in several forms, including pyridinic N, pyrrolic N, graphitic N, and metal-coordinated N species. These nitrogen species have different bonding structures, electron densities, and chemical activities. Therefore, they show different functions during H_2S removal. For example, Edge-N-rich

carbon nanosheet@porous biochar showed that pyridinic N exhibited stronger interaction with H_2S than pyrrolic N and graphitic N. Edge-N species also decreased the energy barriers for H_2S dissociation and O_2 activation [124]. Pyridinic nitrogen is located at the edge of graphitic carbon domains and contains lone-pair electrons. These electrons can coordinate with transition metals and form stable metal-N_X moieties. Such coordination anchors highly dispersed metal species, suppresses particle migration during thermal treatment, and modifies the electronic structure of adjacent metal centers. For example, an axially pyridinic-N-coordinated Ni-N_5 single-atom catalyst showed that the fifth axial pyridinic N ligand increased the electron density of Ni sites and reduced the activation energy barrier for HS intermediate from 2.62 to 1.12 eV. The catalyst achieved an H_2S oxidation activity of 354 $g_S\ kg_{cat}^{-1}\ h^{-1}$ maintained stable catalytic performance for more than 100 h [125]. The important role of pyridinic N was further confirmed in MOF-derived nitrogen-rich hierarchical porous carbon nanofibers (N-PCNFs). The high content of pyridinic and pyrrolic nitrogen, together with hierarchical pores, provided excellent H_2S selective oxidation performance at room temperature (breakthrough sulfur capacity: 3.34 g H_2S/g cat) [103]. Pyrrolic nitrogen mainly affects the electronic environment of defective carbon domains. Because pyrrolic N can donate electrons, it promotes charge redistribution around neighboring carbon atoms and improves the adsorption of polar H_2S molecules. DFT studies showed that pyrrolic N and pyridinic N coordinated with metal atoms produced the highest charge transfer and binding energy among the simulated factors in Zn-MOF-derived N-doped graphitic carbon [112]. Graphitic nitrogen usually improves the electrical conductivity of carbon framework and accelerates electron transport between metal centers and carbon support [126]. This improved conductivity is important for systems involving redox reactions because continuous electron transfer is needed for sulfur oxidation and active site regeneration [103].

The distribution and stability of nitrogen species are strongly influenced by synthesis conditions, particularly pyrolysis temperature and precursor structure. Moderate carbonization temperatures can preserve more pyridinic and pyrrolic nitrogen species. However, higher temperatures can promote their conversion into graphitic nitrogen or cause nitrogen loss. For example, ZIF-8-derived N-doped carbon showed that the total N content decreased from 8.875 atom% at 800 °C to 1.055 atom% at 1100 °C. This change was accompanied by a decrease in pyridinic N and an increase in the degree of graphitization (evidenced by decreasing I_D/I_G ratio) [127]. Graphitization can improve structural stability and electrical conductivity. However, excessive graphitization reduces nitrogen-based coordination sites and decreases the number of available metal-N_X active centers [85,127]. Therefore, nitrogen optimization requires a balance between electronic conductivity and active site availability instead of increasing total nitrogen content.

Future studies should focus on controlling nitrogen configuration and spatial distribution more precisely. Combining operando characterization and theoretical calculations will help clarify how nitrogen species change during sulfur exposure and how they interact with metal centers during repeated adsorption-regeneration cycles.

3.4. Metal-Support Interaction

The catalytic behavior of MOF-based adsorbents is closely related to interfacial interactions rather than only the properties of isolated metal centers [113,128]. Metal-support interaction is an important factor controlling active site stability, sulfur conversion, and regeneration performance [129]. The support is not only a structural framework but also participates in charge transfer, intermediate stabilization, and structural changes during repeated adsorption-regeneration cycles [1,61].

In pristine MOFs, the interaction between metal nodes and organic linkers determines the initial coordination environment of catalytic sites. For example, DFT calculations of MOF-199 showed that copper dimers and trimesic acid (BTC) linkers together form the main adsorption sites for H_2S adsorption at low pressures. H_2S molecules adsorbed on copper sites tend to form a saturated six-coordinated structure [130]. Functional group modification alters this coordination environment by adjusting local electron density. For example, triethanolamine (TEA)-functionalized MOF-199 showed an increased hydroxyl hydrogen from 0.256 to 0.300 after TEA loading. This promoted OH…S interaction with H_2S and increased the adsorption capacity from 1.67 to 2.74 mmol/g [97]. Defect engineering can also modify the coordination environment by exposing coordinatively unsaturated metal sites. For example, benzoic acid-modified MOF-199 generated additional unsaturated Cu sites and changed the coordination structure and electronic properties of Cu^{2+}. As a result, the material achieved sulfur capacities of 69.2 and 78.9 mg S/g for H_2S and CH_3SCH_3 removal, respectively [111]. These observations indicate that H_2S adsorption behavior is determined not only by the identity of the metal but also by the electronic coupling between the inorganic node and its surrounding framework. For example, DFT studies comparing Zn-MOF-74 and Cu-MOF-199 showed that Zn-MOF-74 had stronger CUS binding energy and higher CUS density, while Cu-MOF-

199 showed better desulfurization performance. This indicates that unsaturated metal sites are important for sulfur adsorption, but the interaction between metal centers and linkers also strongly affects the final performance [113].

The role of metal-support interaction becomes clearer after MOF pyrolysis. During thermal conversion, organic ligands are transformed into conductive carbon frameworks containing heteroatom sites and structural defects. At the same time, metal ions are converted into nanoparticles, metal oxides, carbides, or atomically dispersed metal-N_X species [131]. These components remain connected through metal-carbon interfaces, forming complex active structures instead of independent metal particles [30]. Electron transfer across the metal-carbon interface modifies the adsorption energy of H_2S and sulfur-containing intermediates. For example, Co-decorated N-doped hollow carbon nanofibers showed that the interaction between Co species and N-doped carbon promoted electron redistribution, oxygen radical generation, and H_2S activation [123]. In 2D MOF-derived MgO/C heterostructures, defect carbon reduced the energy barrier for $^3O_2$-to-$^1O_2$ activation, while ions and electrons migrate through the water film and carbon substrates promoted redox reactions. This material achieved a high H_2S capacity of 11.2 g/g [109]. The carbon framework also suppresses particle migration. For example, in $Zn_xCo_{3-x}O_4$/CNFs, carbon networks physically separated oxide nanoparticles and inhibited their aggregation [131]. Such interfacial regulation explains the high activity and stability of many MOF-derived carbon materials. For example, $Zn_xCo_{3-x}O_4$/CNFs achieved a sulfur breakthrough capacity of 12.4 g S/100 g sorbent with 83.2% active component utilization [131]. Co@N-doped carbon materials used N-doped graphene to regulate the electron density around Co NPs, which promoted H_2S adsorption and maintained nearly 100% conversion at 190 °C for 28 h [132].

From the perspective of active-site engineering, optimizing the metal-support interaction is no longer limited to maximizing metal dispersion or enhancing metal anchoring. Instead, the goal is to construct a stable interface structure to facilitate efficient charge transfer, while resisting structural degradation in reactive H_2S environments.

3.5. Adsorption vs. Catalytic Conversion

Although both adsorption and catalytic conversion aim to remove hydrogen sulfide, the design principles of the active sites in these two pathways are fundamentally different and should not be confused.

In physical/chemical adsorption, the main goal is to maximize the adsorption capacity and selectivity, which usually relies on strong host-guest interactions. The design considerations include: (i) high-density CUS to achieve strong Lewis acid-base coordination; (ii) microporous structure to enhance binding energy; and (iii) functional groups with acid-base interaction properties (such as -NH_2). In this mode, metals such as nickel (Ni) and zinc (Zn) are often used because they can form stable sulfides, which is beneficial for high-capacity storage, but may also lead to irreversible deactivation.

In catalytic conversion (such as the selective oxidation to produce elemental sulfur), the goal is to convert H_2S into a product that is easy to separate and recover (elemental sulfur), while maintaining reusability. The design focuses on: (i) metal centers with redox activity (such as Cu^+/Cu2$^+$, Fe^{2+}/Fe^{3+}), which can facilitate electron transfer without generating excessive sulfides; (ii) oxygen-activated sites (such as nitrogen-doped carbon-based materials, redox oxides), to provide reactive oxygen species; (iii) moderate sulfur binding capacity to allow for desorption or migration of elemental sulfur; and (iv) hierarchical porous structure to accommodate the volume expansion of sulfur products and facilitate their removal.

It is crucial to distinguish these principles: an excellent adsorbent is not necessarily a good catalyst, and vice versa. Therefore, future material design should be tailored according to the specific operating window, regardless of whether the process is dominated by adsorption or coupled with catalysis.

4. Dynamic Evolution of Active Sites Throughout the H_2S Removal Cycle

4.1. Initial Active Site State

H_2S molecules first diffuse through the pore network and interact with accessible metal centers, heteroatom functionalities, or defect sites. These initial interactions establish the local coordination and electronic environment that subsequently evolves during H_2S activation, sulfur conversion, and regeneration. Dynamic evolution is a conceptual framework that encompasses state-dependent changes, rather than implying that every transformation has been directly observed in real time. Whether H_2S remains molecularly adsorbed, undergoes dissociation, or is directly converted into oxidized sulfur species is largely determined during this early stage [130]. Rather than representing a simple adsorption equilibrium, the initial adsorption process involves simultaneous molecular diffusion, active site recognition, and interfacial electron redistribution (Figure 6) [97,116]. These elementary events collectively determine the accessibility, reactivity, and stability of catalytic sites throughout the adsorption-regeneration cycle [102,119].

The adsorption process starts with the diffusion of H_2S molecules through the hierarchical pore network toward active regions. Wang et al. [102] reported that PVP-regulated hierarchical porous MOF-199 exhibited a lower BET surface area than pristine MOF-199 but had a much larger mesopore volume. The increased mesopore volume allowed more H_2S molecules to access exposed Cu active sites before framework degradation restricted mass transport (Figure 7). Therefore, the optimized MOF-199-P_2 achieved a 34% higher H_2S breakthrough capacity than the original material. This result shows that active site accessibility is mainly controlled by pore connectivity rather than surface area alone. A similar structure-function relationship has also been demonstrated in ZIF-8-derived nitrogen-rich hierarchical porous carbon nanofibers, which achieved efficient H_2S removal at room temperature [103]. These nitrogen sites promoted the selective oxidation of H_2S into elemental sulfur and resulted in a high breakthrough sulfur capacity of 3.34 g H_2S g^{-1} catalyst. After H_2S reaches the adsorption interface, coordinatively unsaturated metal centers generally serve as the primary adsorption sites because their Lewis acidic character enables strong interactions with the lone-pair electrons of sulfur atoms.

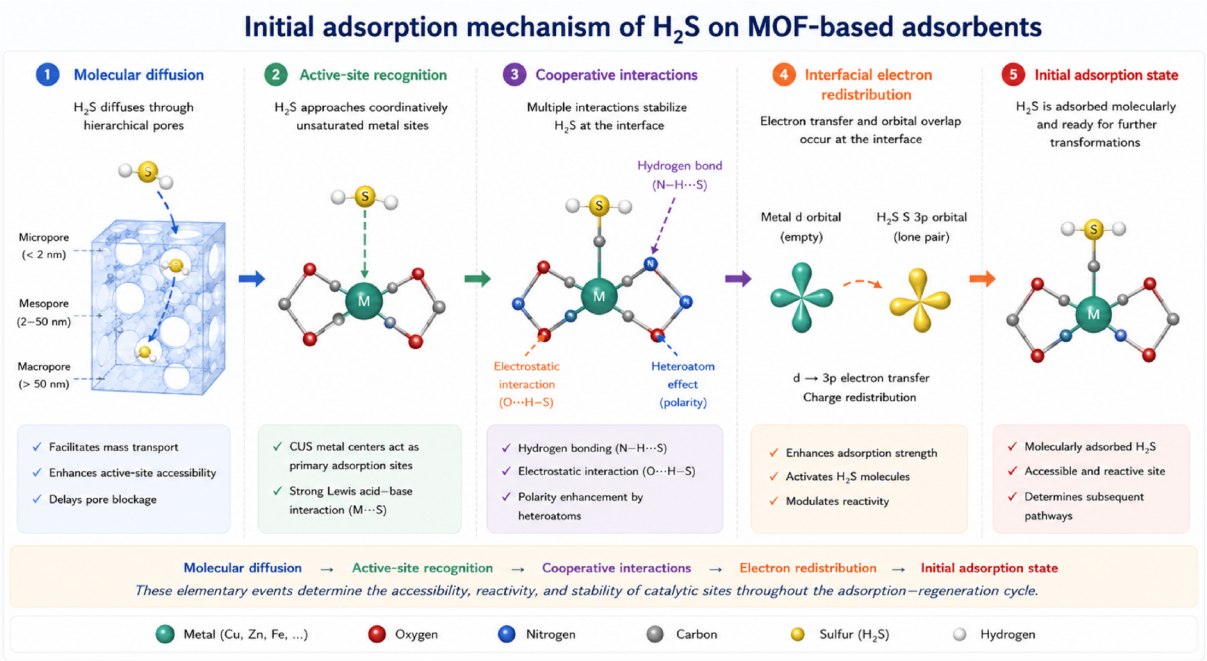


Figure 6. Conceptual diagram illustrating the mechanism of hydrogen sulfide removal by MOF-based adsorbents. The specific adsorption steps and interaction pathways are system-dependent and may vary with material architectures, operating conditions, and atmospheric conditions.

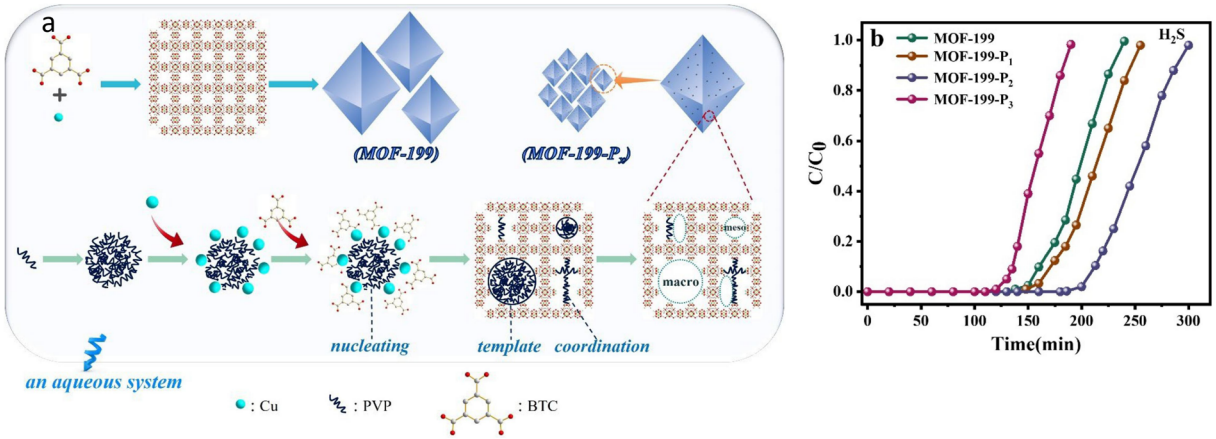


Figure 7. (**a**) The synthesis process of hierarchical porous MOF-199 and role of PVP, (**b**) breakthrough curves on MOF-199 and MOF-199-P$_X$ for H_2S. Reproduced with permission from ref. [102]. Copyright 2022 Elsevier.

Furthermore, the functional groups located on the organic linkers or on the carbon matrix doped with heteroatoms also play a significant role. They actively participate in the adsorption process by forming heterointerfaces, establishing hydrogen bond networks, and altering the local electrostatic environment. This

contribution is evidenced by oxygen-rich MOFs, in which tortuous or "pocket-like" channels provide abundant O sites for favorable electrostatic and dispersion interactions with H_2S [133], and by ZTF/MAF-66, in which H_2S forms relatively strong hydrogen bonds with the nitrogen atoms of the organic linkers [134]. Oxygen-containing groups, amino functionalities, and nitrogen dopants increase the local polarity of the adsorption interface, facilitating molecular enrichment near catalytically active centers, as computationally demonstrated by NH_2-BDC ligands where the amino group increases the polarity in the ligand and enhances its interaction with sulfur, exhibiting acid-base interaction trends with H_2S and physical adsorption character (>−50 kJ/mol) [113], and experimentally confirmed by IRMOF-3 where FTIR analysis reveals a strong $H^{\delta+}\ldots N^{\delta-}$ hydrogen bond between H_2S molecules and the -NH_2 group of the MOF [1]. In heteroatom-doped carbon matrices, replacement of carbon atoms with boron or nitrogen changes the chemical reactivity and forms secondary structures through charge distributions, thereby improving the interaction of polar molecules like H_2S [135].

In another work, Song et al. [30] reported a Cu-MOF-199-derived/N-doped biochar composite. During pyrolysis, the MOF-199/N-doped biochar precursor was converted into an N-doped carbon matrix, with nitrogen supplied primarily by the biochar support, while Cu^{2+} nodes were reduced *in situ* to well-dispersed Cu^0 nanoparticles, creating Cu^0@N-doped carbon heterointerfaces. The reconstructed interface couples Cu^0-mediated O_2 activation with basic sites on N-doped carbon, which promotes the reactive adsorption and oxidation of H_2S, as shown in Figure 8. During H_2S removal, these interfacial active sites work together. Porous carbon enriches H_2S molecules, Cu-based species promote sulfur adsorption and oxidation, and nitrogen species regulate the local electronic structure and stabilize dispersed metal centers.

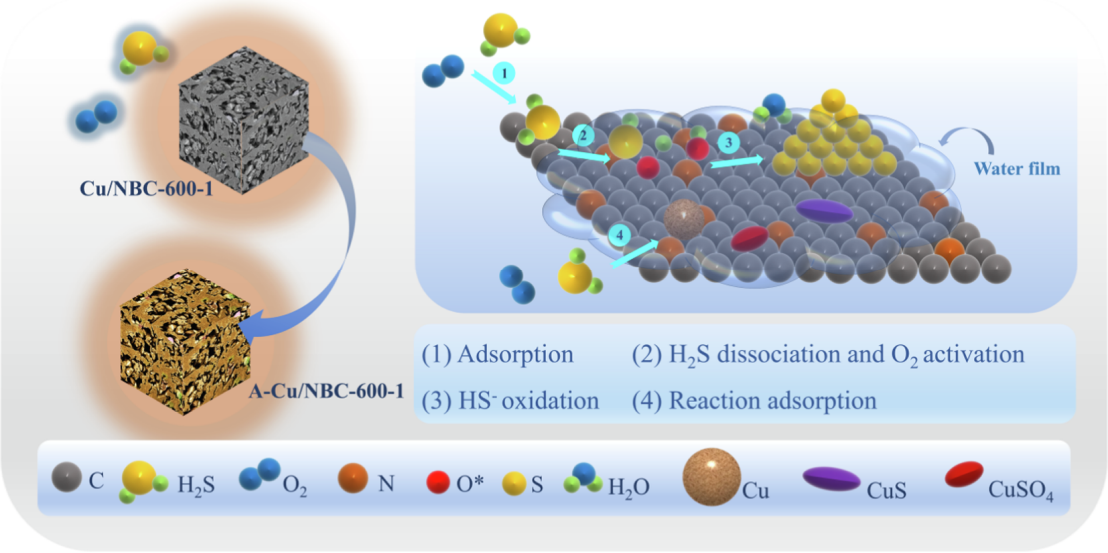


Figure 8. The desulfurization mechanism of H_2S on the Cu-MOF-based adsorbent. Reproduced with permission from ref. [30]. Copyright 2024 Elsevier.

Overall, the initial active sites of MOF-based adsorbents are determined by the accessibility of the metal centers, functional groups of heteroatoms, and pore structure, as well as the coordination environment and spatial distribution. The unsaturated metal sites constitute the main adsorption centers, while the linker or carbon source-derived heteroatom functional groups regulate the local polarity and chemical environment. At the same time, the hierarchical pore structure determines the accessibility and utilization efficiency of these sites. This initial configuration lays the structural and chemical foundation for the subsequent H_2S adsorption and the evolution of active sites during the sulfurization transformation and regeneration process.

4.2. Surface Activation

After molecular adsorption, H_2S enters an activated state on the surface. The S-H bond becomes polarized through charge transfer between H_2S and unsaturated metal centers (CUS) [130]. DFT studies show that electron redistribution during adsorption increases the electrophilic character of hydrogen and the nucleophilic character of sulfur. This process reduces the energy barrier for proton abstraction and converts H_2S into surface hydrosulfide (HS*) species, which are important reactive intermediates in many MOF-based systems [130]. Transition metals with suitable Lewis acidity and accessible redox states provide a good balance between H_2S adsorption and S–H bond activation. For example, Fe^{3+} Lewis acidic sites in MIL-100(Fe) serve as active centers for H_2S adsorption,

dissociation, and oxidation. During this process, Fe^{3+} is reduced to Fe^{2+} and subsequently re-oxidized, completing an Fe^{2+}/Fe^{3+} redox cycle [116]. In UiO-66(Zr/Cu), H_2S adsorption significantly reduces Cu(II) to Cu(I), while emergent S 2p peaks at 161.8 eV (S^{2-}), 163.0–165.3 eV (S^0), and 168.3–169.5 eV (SO_4^{2-}) confirm multiple sulfur intermediates mediated by the Cu^+/Cu^{2+} redox couple [96]. Neighboring μ_3-OH groups facilitate proton transfer and stabilize hydrogen-bonding networks via a proton-extraction mechanism that assists H_2S activation, as suggested by ATR-FTIR of UiO-66(Zr/Cu) where the disappearance of the -OH shoulder peak upon H_2S exposure indicates possible protonation of -OH to $-OH_2^+$ with hydrogen supplied by adsorbed H_2S [96]. In an oxidative environment, the rational design of active sites aims to achieve the selective catalytic oxidation of hydrogen sulfide to elemental sulfur. Activated HS* can react with adsorbed oxygen or lattice oxygen species; however, this path diverges: the optimized catalytic sites promote the coupling of surface sulfur intermediates to form elemental sulfur, while poorly designed sites lead to excessive oxidation and the formation of sulfates. Surface activation refers to the transition from initial adsorption to the reconstruction of dynamic active sites. After H_2S interacts with the active center, changes in charge redistribution, sulfur-hydrogen bond polarization, and metal coordination may alter the local chemical environment. Therefore, the active sites formed after H_2S activation may differ from the original adsorption sites in terms of electronic structure and configuration.

4.3. Adsorption-Induced Active Site Change

The activation of H_2S may significantly alter the electronic and coordination environments of the catalytic center, rather than merely maintaining the initial adsorption sites unchanged. After molecular adsorption and polarization of the sulfur-hydrogen bond, the sulfur-containing intermediates may change the local coordination structure and electronic state of the metal center. These changes caused by adsorption will affect the conversion efficiency of sulfur and the reversibility of the subsequent regeneration process, highlighting the state-dependent characteristics of the active sites in MOF adsorbents [60].

A key feature of this evolutionary process is the change in the electronic state of the metal during the H_2S activation process. It should be stressed that reversibility is not a general attribute of this step. In several of the systems discussed below, the evidence is limited to endpoint (pre- and post-exposure) comparison rather than time-resolved tracking of the same site, and in strongly sulfidizing systems the change is effectively irreversible. The coordinatively unsaturated metal center can participate in redox reactions, resulting in a redistribution of electron density and the formation of a new catalytic configuration. For copper-based MOFs, exposure to H_2S triggers Cu-S coordination and changes in the oxidation state of Cu [60]. Similar redox flexibility was also observed in the copper-based porous coordination network, where the adsorption of H_2S promoted the interconversion between Cu^+ and Cu^{2+}, and was accompanied by the formation of sulfur-containing intermediates [118]. Iron-based MOFs exhibit similar behaviors, where the coexistence of Fe^{2+}/Fe^{3+} sites enables reversible electron transfer during the activation and oxidation of H_2S (Table 4) [116,136]. These studies indicate that the catalytic performance is closely related to the interconversion between different metal oxidation states, rather than solely depending on a single optimal oxidation state.

Table 4. Comparison of active sites and H_2S removal mechanisms in representative MOF-based materials.

Material	Active Site	Initial H_2S Interaction	Sulfur Species	Active Site Evolution	Ref.
CuBTC	Cu^{2+} CUS	Cu-S coordination	CuS/SO_4^{2-}	$Cu^{2+} \rightarrow Cu^+$	[60]
MIL-100(Fe)	Fe^{2+} CUS	H_2S activation	S^0/SO_4^{2-}	Fe^{3+}/Fe^{2+} cycling	[116]
UiO-66(Fe/Zr)	Fe-Zr node	Adsorption-dissociation	S^0/SO_4^{2-}	Fe^{3+}/Fe^{2+} redox cycling	[110]
Cu/NBC	Cu nanoparticles + N sites	Adsorption-oxidation	$CuS/S^0/SO_4^{2-}$	Metal-carbon interface reconstruction	[30]

In addition to electronic reconstruction, the exposure of sulfur can directly alter the coordination environment of the metal center. In CuBTC, the adsorption of H_2S will cause partial dissociation of the Cu-carboxyl bond and the formation of Cu-S interactions, while also resulting in a decrease in crystallinity and a reduction in surface accessibility [60]. Moderate structural adaptation may generate more reactive sulfur-associated configurations, whereas excessive sulfur coordination can occupy accessible metal centers and result in irreversible deactivation.

Operando and *ex situ* characterization studies further reveal that variations in metal valence states and coordination structures often occur before significant capacity loss, suggesting that deactivation originates from cumulative structural evolution rather than instantaneous active site poisoning [60,118].

4.4. Roles and Possible Evolution of Nitrogen Functionalities

Nitrogen functionalities act as active electronic regulators for metal-centered H_2S activation, rather than only structural components. During H_2S adsorption, electron transfer between metal sites and H_2S can extend to the surrounding nitrogen-doped carbon matrix. The lone-pair electrons of pyridinic N alter the local charge distribution and influence H_2S adsorption [137].

NaCl-templated N-doped porous carbon (NC-10-800) showed high H_2S removal performance. The high pyridinic N content and carbon defects provided Lewis base sites for H_2S adsorption and dissociation, resulting in a sulfur formation rate of 784 $g_S\ kg_{cat}^{-1}\ h^{-1}$ with >100 h [138]. In Co@N-doped carbon, DFT calculations show that N-doped graphene regulated electron density around Co nanoparticles and promoted H_2S adsorption [132].

Nitrogen-enriched defective carbon domains can change the adsorption energies of HS*, S*, and oxygen-containing sulfur species through electronic effects. This regulation controls the residence time of sulfur intermediates on the catalyst surface [138]. Appropriate charge redistribution facilitates the migration and subsequent conversion of these intermediates. However, excessive sulfur binding may block nearby active sites and reduce regeneration efficiency [138]. Therefore, nitrogen functionalities not only stabilize metal species but also regulate sulfur species during the whole reaction process.

Nitrogen, metal species, and carbon defects form an interconnected electronic network that changes with the chemical environment created during H_2S adsorption and sulfur conversion.

4.5. Sulfur Conversion and Active Site Deactivation

H_2S activation first produces highly mobile HS* and S* intermediates that remain close to metal centers. These sulfur species can be further oxidized or coupled to form elemental sulfur, polysulfides, sulfites, or sulfates depending on oxygen availability and the redox properties of the catalyst [60]. This dynamic competition between sulfur conversion and accumulation governs whether catalytic activity can be restored.

During sulfur deposition, sulfur-containing species gradually occupy the coordination sites of metal centers and block active sites. In CuBTC, H_2S interaction breaks Cu-carboxylate bonds, causing a 65% drop in surface area and 49% loss in pore volume after adsorption. Sulfate species are especially difficult to remove. For example, in Fe_2O_3/TiO_2 catalysts, elemental sulfur and sulfate deposition are identified as the main reasons for deactivation [139]. Ce-Mn oxide nanocomposites mitigate this issue by leveraging strong Ce-Mn interaction and abundant surface-active oxygen species. These features promote sulfur formation and inhibit sulfate accumulation during reaction [140]. Therefore, catalyst lifetime is not only related to the total amount of sulfur deposited but also depends on the change of sulfur species during repeated operation.

The distribution of sulfur inside the material is also important. In hierarchical porous MOF-199 regulated by PVP, H_2S adsorption is chemical and induces structural collapse. However, the hierarchical pore structure enables H_2S to access maximal active sites before pore blockage occurs. As a result, MOF-199-P_2 achieved an optimal breakthrough capacity 34% higher than the bare framework [102]. This result shows that interconnected pore structures can facilitate H_2S diffusion and delay diffusion-related deactivation. MOF-199@1%ACF further reveals the staged nature of sulfur accumulation. H_2S first adsorbs on the external surface and then diffuses into micro/mesopores. Inside the pores, H_2S dissociates into HS^- through a surface water film. The generated sulfur species are then oxidized into elemental sulfur or react with Cu^{2+} to form CuS [141].

Overall, the removal process of hydrogen sulfide involves the gradual transformation of active sulfur intermediates into elemental sulfur, metal sulfides, and sulfates, accompanied by continuous changes in the local environment of the active sites. The accumulation of these sulfur species will clog the coordination sites and channels, alter the coordination mode of the metals, and gradually reduce the accessibility and reactivity of the sites. Thus, the conversion of sulfur and the deactivation of the active sites are a closely coupled process, which ultimately determines the long-term performance of the MOF adsorbents in cyclic operation.

4.6. Environmental Effects

The removal of industrial-grade hydrogen sulfide is rarely carried out under idealized single-component conditions. Actual gas streams, such as biogas, natural gas, and coke oven gas, not only contain H_2S but also contain large amounts of competing gases (such as CO_2, CH_4, CO) as well as a high content of water vapor [142]. In biogas and landfill gas, CH_4 and CO_2 are the two dominant constituents, typically accounting for 50–80 vol% and 20–50 vol%, respectively, whereas H_2S is present only at trace levels, commonly 100–1500 ppmv in agricultural biogas and reaching up to 12,000 ppmv in landfill gas [143]. These environmental factors have a profound impact on the dynamic evolution of active sites, often determining whether the adsorption capacity, catalytic performance, and structural integrity of the material can be maintained under actual operating conditions.

Water molecules are strong Lewis bases and can compete with many unsaturated metal sites in metal-organic frameworks for coordination. These unsaturated metal sites are the main active centers for H_2S binding. For structures sensitive to water, such as HKUST-1 (Cu-BTC) [144], exposure to a humid environment can lead to progressive structural degradation: water molecules replace the organic linkers through the hydrolysis of metal-ligand bonds, causing the crystal structure to collapse and irreversibly losing the unsaturated Cu^{2+} sites. In contrast, water-stable MOFs such as UiO-66(Zr) possess a highly stable metal node connection structure ($Zr_6O_4(OH)_4$ clusters, containing strong Zr-O bonds), enabling them to maintain the pore structure and accessible active sites even under high humidity conditions [145]. However, water stability alone does not guarantee the best hydrogen sulfide removal performance. In UiO-66, water molecules may still occupy the open Zr sites and compete with H_2S for adsorption, thereby reducing the effective sulfur capacity.

More importantly, from the perspective of dynamic active-site engineering, humidity may have a dual effect. On the one hand, excessive moisture can lead to irreversible structural degradation (as shown in HKUST-1), after regeneration at 200 °C, the H_2S/CO_2 selectivity of HKUST-1 fell from 5.28 to 0.27; on the other hand, the thin water film formed on the pore surface can facilitate the decomposition of H_2S into HS^- and H^+ [141], thereby promoting surface activation and triggering subsequent catalytic oxidation reactions. This duality highlights the need to distinguish between the framework collapse caused by water and the reaction pathways assisted by water when designing renewable adsorbents.

The influence of competitive gases (CO_2, CH_4, CO) should also be considered. During the capture of H_2S, CO_2 is a relatively competitive gas because both of these molecules are acidic and can interact with basic sites or open metal centers. In metal-organic framework materials modified with amino functional groups (such as UiO-66-NH_2 [57], MIL-125(Ti)-NH_2 [43,59]), CO_2 can react with amino groups to form carbamates or bicarbonates, directly competing with H_2S for the same adsorption sites. This not only reduces the adsorption amount of H_2S but also changes the local electronic environment, possibly inhibiting the dissociation of H_2S. In contrast, the unmodified UiO-66 exhibits poor H_2S/CO_2 selectivity, with an H_2S uptake of only 0.057 mmol/g, because it lacks active sites with strong selectivity; while UiO-66 with defect engineering that exposes Zr sites can preferentially adsorb H_2S rather than CO_2, because there is a stronger interaction between sulfur and Zr. Since methane (CH_4) is non-polar and chemically inert, it usually has less competitive interaction with H_2S at open metal sites [64]. In certain industrial gas streams, extremely low concentrations of carbon monoxide (CO) can combine on metal centers with redox activity (such as Cu^+, Fe^{2+}/Fe^{3+}), thereby interfering with the redox cycling process necessary for the catalytic oxidation of hydrogen sulfide [146].

To address the challenges posed by the composition of real gases, future dynamic active-site engineering should consider the following points: (i) enhance the covalency of metal-ligand bonds (such as Zr-O) to improve the resistance to hydrolysis; (ii) introduce hydrophobic functional groups or hierarchical pore networks, which can both exclude a large amount of water and allow H_2S to diffuse; (iii) design sites based on the hard-soft acid-base principle with high selectivity for H_2S/CO_2; and (iv) utilize MOF-derived materials in which the carbon support may protect the active sites from water erosion while maintaining their chemical reactivity.

In summary, the evolution path of hydrogen sulfide on MOF materials is highly dependent on the operating environment, especially the gas atmosphere, humidity, and the properties of the active sites (Figure 9). Under relatively dry and inert conditions, hydrogen sulfide is more likely to undergo molecular adsorption or coordinate with accessible metal centers, resulting in limited sulfur conversion. When oxygen is present, the redox-active metal sites and metal-heteroatom interfaces can promote the oxidation of sulfur intermediates to elemental sulfur. Increased humidity may further alter the adsorption environment through the introduction of water-mediated hydrogen bond interactions and competitive occupation of active sites; in some systems, surface water is conducive to the dissociation of hydrogen sulfide and subsequent sulfur conversion. When exposed to strong sulfurophilic metal sites, prolonged contact with hydrogen sulfide may instead promote the coordination of the metal with sulfur and the formation of metal sulfides, which often leads to irreversible blocking of the sites and more difficult regeneration. Therefore, the main sulfur-containing products can range from molecularly adsorbed H_2S/HS^- to elemental sulfur, and then to oxidized sulfur species such as sulfites or sulfates under stronger oxidation conditions. These condition-dependent conversion paths indicate that the removal of hydrogen sulfide should not only consider its adsorption capacity but also take into account the relationship between the operating environment, humidity, the properties of active sites, and the distribution of sulfur oxidation states.

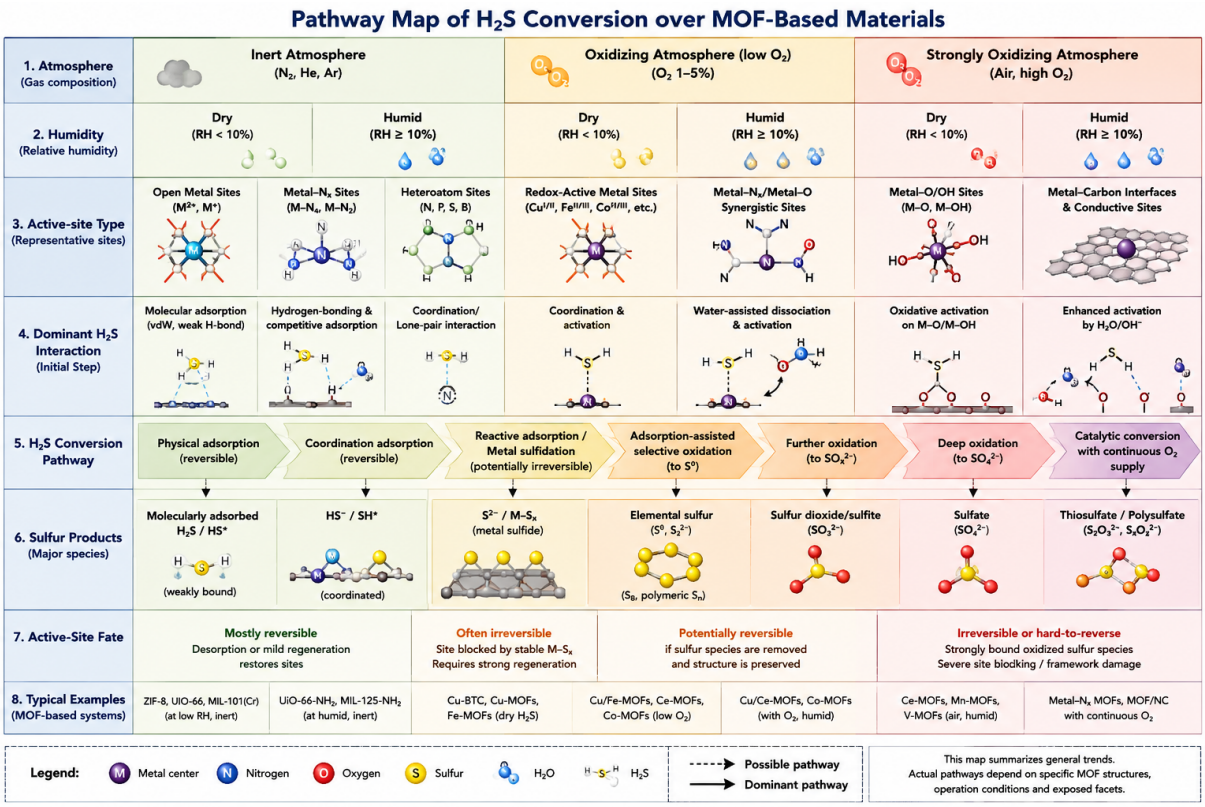


Figure 9. Conceptual diagram illustrating the pathway map for H_2S reaction networks. The depicted conversion pathways and sulfur products, together with the regime boundaries (including relative humidity) and the reversible/irreversible assignments, are indicative and system-dependent rather than universal.

5. Regeneration and Active Site Recovery

From the perspective of dynamic active-site engineering, regeneration is not merely the removal of adsorbed sulfur species. It also implies the reverse or partial reconstruction of the coordination, electronic structure, and interface configuration of the active sites after sulfur exposure. Therefore, when evaluating the effectiveness of a regeneration strategy, it should not only be based on the recovery of H_2S capacity, but also consider its ability to restore the accessibility, chemical state, and structural integrity of the active sites.

5.1. Thermal Regeneration

Thermal regeneration is one of the most commonly used methods to recover the adsorption performance of MOF-based H_2S adsorbents because it is simple to operate and can be easily applied in fixed-bed desulfurization systems. During this process, high temperatures promote the decomposition, desorption, or oxidation of sulfur-containing deposits. Recent studies show that thermal treatment can also cause significant changes in catalytic interfaces [147].

The efficiency of thermal regeneration mainly depends on the type of sulfur species formed during adsorption. Weakly bound elemental sulfur can usually migrate or volatilize under moderate heating, which helps reopen blocked pore channels [60]. However, stable metal sulfides require oxidation or decomposition before active metal centers can be recovered [128]. Sulfate species generally exhibit even higher thermal stability and often persist after conventional heating. This leads to incomplete regeneration and gradual loss of adsorption during repeated cycles [128]. Therefore, regeneration efficiency is controlled not only by regeneration temperature but also by the sulfur speciation during adsorption.

The supporting framework also undergoes structural evolution during regeneration. In pristine MOFs, repeated heating may weaken coordination bonds between metal nodes and organic linkers. Among eight representative MOFs, only UiO-66(Zr), MOF-801(Zr), and MOF-74-Mg exhibited reversibility, albeit with limited capacity (≤3.81 mg/g), whereas MOF-199-Cu, ZIF-8-Zn, MOF-74-Ni, MIL-101(Cr), and MOF-74-Zn suffered framework collapse upon H_2S exposure [53]. For the four CUS-bearing frameworks, this collapse is attributable to the strong interaction between open metal sites and H_2S; ZIF-8-Zn, by contrast, degraded despite its nominally saturated tetrahedral Zn sites, indicating that H_2S can attack the framework through linker displacement even when

no open coordination site is available. By comparison, MOF-derived carbons and hybrid composites generally exhibit greater resistance to thermal cycling. Sep/Cu-BDC nanocomposite regenerated at 190 °C under N_2 flow for 4 h maintained excellent recyclability over three consecutive cycles [148]. The cycling performance of representative MOF H_2S materials upon multiple regeneration cycles is summarized in Table 5. Cycle number, regeneration conditions, and capacity retention are the quantities most consistently reported and provide a direct basis for comparing active site stability under repeated exposure and regeneration. Because most of these measurements were made on powder samples under simplified gas streams, the retention values primarily reflect intrinsic site stability rather than process performance. Scalable synthesis, shaping and mechanical robustness, pressure-drop control, heat management, and process economics are rarely addressed in the same studies, and reporting them alongside the cyclic metrics would allow these materials to be assessed for process feasibility as well.

Table 5. Cyclic H_2S removal and regeneration performance of representative adsorbents.

Sample	C_t/C_0 (%)	Regeneration Method	Regeneration Conditions	Regeneration Duration (h)	Cycle (s)	Relative Capacity (%)	Ref.
3DOM-SC-43-NH_3	0.2	Thermal regeneration	650 °C; air	2	5	29	[149]
Cu-BTC	1	Thermal regeneration	160 °C; air	2	1	18	[54]
Fe-Cu-BTC	1	Thermal regeneration	160 °C; air	2	6	18	[54]
UiO-66-NH_2	100	Thermal regeneration	200 °C	/	2	42	[57]
MIL-101-Cr	100	Thermal regeneration	200 °C; N_2	12	3	15	[53]
MOF-199-Cu	100	Thermal regeneration	200 °C; N_2	12	3	14	[53]
MOF-74-Ni	100	Thermal regeneration	200 °C; N_2	12	3	37	[53]
MOF-74-Zn	100	Thermal regeneration	200 °C; N_2	12	3	21	[53]
MOF-199	100	Thermal regeneration	70 °C	48	3	58	[129]
Ag-Cu-MOF	20	Chemical regeneration	0.065 mol/L H_2O_2	/	5	14	[150]
Cu-based MOF	100	Chemical regeneration	Soaking in DMF solvent	/	1	95	[118]
Dry CuBDC	80	Chemical regeneration	Methanol + UV; N_2	28	1	19	[60]
Moist CuBDC	80	Chemical regeneration	Methanol + UV; N_2	28	1	30	[60]
Dry CuBTC	80	Chemical regeneration	Methanol + UV; N_2	28	1	38	[60]
Moist CuBTC	80	Chemical regeneration	Methanol + UV; N_2	28	1	237	[60]
ZnBTC-ZnO	>80	Chemical regeneration	Methanol + UV; N_2/O_2	76	1	46	[128]
$Cu(BDC)_{0.5}(BDC\text{-}NH_2)_{0.5}$	10	Chemical regeneration	Methanol + UV; N_2/O_2	8	4	8	[35]

Note: Relative capacity is calculated as the regenerated H_2S capacity relative to the fresh-material capacity under the corresponding conditions. Values above 100% indicate that the regenerated material exhibited a higher capacity than the fresh material.

From the perspective of energy consumption, thermal regeneration typically requires a temperature range of 160 to 650 °C (Table 5), while removing sulfates requires even higher temperatures. Although metal-organic framework materials suitable for thermal regeneration can withstand moderate heating, the energy input required for continuous high-temperature operation is relatively large, especially in large-scale fixed-bed systems. For example, for a 1 kg bed with a purge at GHSV 500 h^{-1}, heating the adsorbent itself from 25 to 200 °C consumes only ~0.05 kWh ($c_p \approx 1.0$ kJ kg^{-1} K^{-1}), whereas heating the purge gas over the 12 h hold typical of Table 5 consumes ~0.76 kWh, roughly fifteen times more. The energy penalty of thermal regeneration in these systems therefore resides in the duration of the isothermal purge rather than in the peak temperature. It reframes the

optimization target: shortening the hold time is worth more than lowering the set-point. Moreover, the regeneration atmosphere further influences active site recovery. Oxidative atmospheres facilitate conversion of metal sulfides into catalytically active oxides while accelerating oxidation of elemental sulfur into volatile sulfur oxides [150]. However, excessive oxidation may over-oxidize active metals or generate thermally stable sulfate species that are difficult to remove in subsequent cycles [129]. Inert atmospheres minimize oxidation-induced structural degradation but are generally less effective for decomposing strongly bound sulfur compounds [60]. Therefore, the thermal regeneration performance should take into account the three factors: temperature (energy consumption), atmosphere and catalyst, rather than just the heat energy itself.

5.2. Chemical Regeneration

Chemical regeneration includes solvent washing (e.g., methanol, DMF), redox-mediated extraction, and photo-assisted treatments. It provides another method to recover the activity of sulfur-saturated MOF-based adsorbents under mild conditions. These reactions can also modify catalytic interfaces and restore the electronic and coordination environments needed for efficient H_2S activation [60].

Solvent- and photo-assisted chemical regeneration has been most extensively demonstrated in copper-based MOFs. Methanol washing combined with low-power UV-C irradiation enables the successive removal of physically adsorbed H_2S and the generation of new binding sites [60]. For spent CuBTC, this treatment reduces sulfur content from 3.91 at% to 1.49 at%, repositions Cu 2p peaks close to those of the fresh MOF, and recovers the surface area from 110.9 to 410.8 m^2/g, even higher than the fresh value of 317.0 m^2/g [60]. Consequently, the regenerated CuBTC delivers an exceptional adsorption capacity of 95.6 mg/g in the second cycle, 2.37-fold that of the fresh material, which is linked to the reactivation of Cu sites and improved porosity [60]. Similarly, Zn-MOF/ZnO nanocomposites regenerated by the successive effect of methanol and UV irradiation exhibit decreased sulfur content and decreased Zn ionic character, leading to increased adsorption capacity in the second cycle [128]. In mixed-ligand $Cu(BDC)_{0.5}(BDC\text{-}NH_2)_{0.5}$, methanol/UV treatment partially regenerates spent adsorbent, where spectroscopic analysis predicts Cu(OH)-type sites after UV irradiation accompanied by increased surface area, which are responsible for the enhanced adsorption capacity of the regenerated sample [35].

The regeneration chemistry also governs sulfur speciation and metal-site recovery. In bivalent Cu-MOFs such as PCN-6-M, adsorbed H_2S is mineralized to sulfide, sulfur, and sulfates mediated by the Cu^+/Cu^{2+} redox cycle in the presence of adsorbed water and molecular oxygen; the material can be partially recovered after soaking in DMF solvent, confirming that solvent environment actively modulates metal valence states and interfacial electron distribution [118]. This demonstrates that chemical regeneration functions do not only remove sulfur species but also regulate metal oxidation states and coordination environments.

Chemical regeneration has been proven to achieve significant results in partially restoring the sulfur-loaded MOFs, and even in some cases outperforming the capacity of fresh materials [60]. However, this process requires treatment times of 8–76 h [128], considerably longer than those of most thermal protocols, which generally require 2–12 h, although a 48 h treatment has also been reported (Table 5), and generates liquid waste that must be disposed of or recycled. Moreover, the solvent is difficult to fully penetrate into the micropores, limiting the regeneration efficiency of the high-density sulfide framework. In CuBDC, methanol/UV treatment recovers only 32% of the fresh capacity because most Cu sites remain bound to sulfide and cannot be regenerated [60]. $Cu(BDC)_{0.5}(BDC\text{-}NH_2)_{0.5}$ likewise undergoes only partial regeneration, as H_2S breaks Cu-carboxylate bonds to form covellite CuS nanoparticles and sulfates that are difficult to completely remove [35]. Therefore, although the chemical regeneration conditions are mild, which does not necessarily imply a lower overall burden: its scalability is constrained by the solvent consumption, treatment time, and incomplete removal of sulfides. Crucially, no study reports solvent consumption per cycle (L per kg of adsorbent), the sulfur content of the spent liquor, or the energy required for solvent recovery by distillation, so its advantage over thermal regeneration cannot presently be quantified.

In summary, whether it is thermal regeneration or chemical regeneration, under the cumulative effect of multiple adsorption-desorption-regeneration cycles, gradual structural degradation may occur, particularly in water-sensitive or strongly sulfidizing MOFs. Neither combines low energy demand, short duration, high-capacity retention, and an acceptable waste stream. Each cycle causes the MOF framework to repeatedly endure thermal stress, chemical erosion (such as hydrolysis, sulfur poisoning), and mechanical strain caused by changes in pore volume. For MOF materials sensitive to water (such as HKUST-1), even with only trace amounts of water during the cycling process, the hydrolysis of metal-ligand bonds will accelerate, leading to irreversible loss of the lattice structure and a decrease in the accessibility of active sites. Similarly, in MOFs where active sites undergo dynamic reconfiguration during H_2S desorption (such as bond breakage and reformation initiated by sulfur), after repeated cycles, they may transform into a thermodynamically stable but catalytic activity-lacking bulk phase (such as metal

sulfides or sulfates). This cyclic degradation is usually more severe than single-stage deactivation because it means that the dynamic active site resources of the material are completely exhausted. Without a robust structural design, it will not be possible to achieve long-term industrial application.

6. Characterization Strategies for Resolving Active Site Evolution

Understanding MOF-based H_2S adsorbents requires monitoring the changes of active sites during adsorption, sulfur conversion, and regeneration. Traditional *ex situ* analysis only compares fresh and used materials, which cannot capture short-lived intermediates or changes at interfaces. This knowledge gap has driven the broader use of complementary *ex situ* and *in situ* characterization techniques, including vibrational spectroscopy (Raman, DRIFTS), X-ray photoelectron spectroscopy (XPS), X-ray diffraction (XRD), while operando X-ray absorption spectroscopy (XAS) remains underutilized in H_2S-MOF systems. DFT calculations provide atomic-level information about H_2S adsorption structures, Cu-S bond formation, and the thermodynamic stability of different sulfur species (S^{2-}, S^0, SO_4^{2-}). These calculations help connect spectral results with changes in electronic structures.

Ex situ spectroscopy provides useful information on sulfur species and metal valence changes before and after reaction. In CuBTC, methanol/UV regeneration moves Cu 2p peaks closer to the fresh CuBTC sample and recovers the low-angle XRD intensity. These results indicate partial recovery of the Cu electronic environment and framework structure. However, they do not directly prove complete reversible reconstruction of the material [60]. Similar Cu^+/Cu^{2+} redox cycling mediating H_2S mineralization has been observed in bivalent Cu-MOFs (PCN-6-M), where adsorbed H_2S is converted to sulfide, sulfur, and sulfate species [118]. These *ex situ* XPS/XRD sequences, although not strictly operando, allow comparison of interfacial states before H_2S exposure, after exposure, and after regeneration, but do not directly resolve their temporal evolution.

In situ monitoring offers more direct temporal resolution. In Cu-MOF-derived Cu/NBC-600-1, *in situ* DRIFTS recorded under 25 °C, 70% relative humidity, and 20% O_2 reveals that vibrational peaks attributable to sulfate species increase continuously over time, supporting the progressive formation of oxidized sulfur species at the catalyst surface [30]. In HKUST-1, diffuse reflectance DRUV-Vis-NIR spectroscopy during H_2S exposure (20 mbar) captures a real-time shift of the ligand-to-metal charge transfer (LMCT) band to ~470 nm and a blue-shift of the d-d band to ~687 nm with decreased intensity, indicating that the coordination sphere of copper is strongly perturbed upon H_2S interaction [61]. Together with the FTIR, Raman, and powder X-ray diffraction (PXRD) results, these optical changes indicate progressive perturbation of the Cu coordination environment and the eventual formation of covellite CuS at higher H_2S pressures [61].

XAS can extend this capability to coordination geometry. The sensitivity of XAS to short-range atomic order makes it particularly suitable for MOF-derived materials where long-range crystallinity is partially lost [60]. However, the CuBTC and $Cu(BDC)_{0.5}(BDC\text{-}NH_2)_{0.5}$ regeneration results discussed above were obtained from XPS, XRD, and surface-area measurements rather than XAS and therefore should not be presented as XAS evidence. Within the literature reviewed here, genuinely operando XAS studies of H_2S removal by MOF-based materials remain scarce. XAS is therefore better positioned as a promising but underutilized method. Future studies should correlate X-ray absorption near-edge structure (XANES) edge and white-line changes and extended X-ray absorption fine structure (EXAFS)-derived coordination numbers and M-S bond distances with simultaneous H_2S breakthrough, conversion, or product-formation data under working conditions.

Density functional theory has also become a powerful tool for elucidating the atomistic mechanism of H_2S adsorption, sulfur accumulation, and regeneration. For example, Zhang et al. [107] studied the valence state evolution of sulfur on UiO-66 through the DFT method and identified a stepwise path: $H_2S \rightarrow HS^* \rightarrow S^* \rightarrow S_8$. During this process, H_2S is selectively oxidized to multiple sulfurs. Chen et al. [113] used DFT calculations to reveal the energy barriers corresponding to the sulfur removal during thermal regeneration and oxidative regeneration processes. They pointed out that the metal centers in MOFs have different binding strengths for sulfur species, with Fe-CUS > Cu-CUS > Zn-CUS. This fundamentally determines the differences in the stability of the generated metal sulfide phases. For Cu-MOFs, experimental studies have shown that the CuS formed upon exposure to H_2S can be (partially) reversed by annealing at relatively low temperatures (approximately 180 °C under N_2 protection) [107]. Therefore, these calculation methods can provide an in-depth understanding of the reversibility and irreversibility of the transformation of active sites at the atomic level.

MOFs and their derived materials possess a vast chemical space, making it difficult to conduct comprehensive experimental screening. Machine learning (ML) offers a data-driven alternative for rapidly predicting H_2S adsorption performance and guiding material design. Tree-based ensemble methods, such as Random Forest (RF) and Extreme Gradient Boosting (XGB), and Light Gradient Boosting Machine (LGBM) are commonly used algorithms for MOF adsorption studies that are particularly effective in feature importance analysis [151]. They

can identify which structures or chemical descriptors (such as pore volume, metal electronegativity, nitrogen content) have the strongest correlation with gas adsorption capacity. For example, a recent study utilized a dataset containing 676 entries to develop five ML models to correlate the characteristics of adsorbents, adsorption conditions, and adsorbate characteristics with the influencing factors that affect the sulfur adsorption capacity of MOF samples [152], but it was constructed for the liquid-phase adsorptive desulfurization of thiophenic compounds (benzothiophene, dibenzothiophene, and 4,6-dimethyldibenzothiophene) from model fuel, not for gas-phase H_2S. Of the five algorithms compared, the multilayer perceptron performed best (test MSE 0.0032), whereas the random forest model was the weakest (test MSE 0.0045), which the authors attributed to overfitting. Two of these findings are nevertheless instructive for H_2S. First, the dominant descriptors were process variables, with SHAP values of 0.51 and 0.37 for initial sulfur concentration and contact time, respectively, whereas the authors reported that adsorbent structure accounted for approximately 36% of the overall contribution. These values are reported according to the metrics used in the original study and should not be interpreted as directly normalized quantities on the same scale. Second, the optimized material (Zr-MOF, 5.96 nm pores) reflects the steric demands of polycyclic thiophenes and is not transferable to H_2S. Current models largely encode operating conditions rather than material design rules, and contain no descriptor for the state-dependent active site properties, such as redox accessibility, coordination flexibility, sulfur-binding energetics; these properties govern H_2S capture and regeneration. A H_2S-specific dataset including such dynamic descriptors is therefore a prerequisite, not an optional refinement. Studies that do address H_2S directly remain scarce, but they demonstrate the feasibility of this route. He et al. [153] utilized an RF model to efficiently identify and design MOF materials with excellent H_2S/CH_4 separation performance from a vast MOF database.

In summary, no single technique captures how active sites change during H_2S removal, so the methods are ranked by how directly they observe it. Comparing fresh and spent samples (*ex situ* XPS/XRD) shows which states a site can reach, but not whether it returns the same way. Repeating this after each regeneration shows whether a state reappears, supporting apparent reversibility. *In situ* DRIFTS and DRUV-Vis-NIR, with XAS under the reacting gas, follow intermediates as they form. Operando measurement, recorded simultaneously with breakthrough or conversion, gives the strongest evidence, because it links a structural change to performance under working conditions; this is the basis on which reversibility is assigned. Static DFT and ab initio molecular dynamics (AIMD) test whether a pathway is feasible; they do not observe it. When appropriately integrated, these approaches can establish a more defensible correlation between spectral signatures, coordination changes, sulfur speciation, and adsorption-regeneration performance, thereby strengthening the mechanistic foundation for dynamic active site engineering.

7. Future Perspectives

Significant progress has been made in developing MOF-based H_2S adsorbents. However, current research still mainly depends on experimental optimization rather than mechanism-guided design [1]. This review shows that removal performance is controlled not only by the properties of individual active sites but also by their state-dependent changes during adsorption, sulfur conversion, and regeneration [60]. Future research should move from constructing highly active materials toward understanding and controlling dynamic catalytic interfaces operating under realistic reaction environments.

One important challenge is to develop quantitative descriptors that connect active site changes with adsorption performance. Current studies commonly evaluate catalyst activity based on equilibrium adsorption capacity or breakthrough time. However, changes in metal valence, coordination environment, sulfur species, and interfacial electron distribution during operation are rarely considered [60]. As demonstrated throughout this review, active sites can change under reaction conditions, and these transient states frequently determine catalytic behavior more strongly than the initial catalyst structure. Future studies should focus on operationalizing dynamic descriptors (Table 6), including metal redox behavior, coordination flexibility, sulfur-binding energetics, sulfur speciation and interfacial charge transfer. These descriptors can connect atomic-scale changes with overall adsorption performance [44]. They can also provide a common method to compare different MOF-based adsorbents and support mechanism-based material design.

Artificial intelligence (AI) offers new opportunities for faster catalyst development [154]. Traditional MOF design mainly relies on repeated synthesis and experimental testing. This process becomes less efficient as the composition and structure of MOFs become more complex [154]. Data-driven methods can improve this process by combining computational results, experimental databases, and machine-learning algorithms. Future AI models should incorporate descriptors directly related to dynamic active site evolution, including metal redox accessibility, sulfur-binding energetics, coordination flexibility, and interfacial electron redistribution [155]. Combining DFT

calculations with graph neural networks, Bayesian optimization, and autonomous experimentation could enable inverse design of MOF architectures possessing desired dynamic reconstruction characteristics [154]. In addition, adding operando characterization data into machine-learning models can help predict how catalysts change during adsorption-regeneration cycles instead of only using initial structural information [44]. Such closed-loop platforms combining computation, artificial intelligence, and automated synthesis are expected to transform catalyst development from trial-and-error optimization to predictive materials engineering.

Table 6. Operationalization of dynamic active-site descriptors for MOF-based H_2S adsorbents.

Descriptors	Operational Definition	How to Obtain
Redox accessibility	Fraction of metal centres returning to the pristine oxidation state after regeneration	XPS/XAS
Coordination flexibility	Reversible change in metal coordination number/bond length	EXAFS/AIMD
Sulfur-binding energetics	E_{ads} of H_2S, HS, S at the site	DFT
Sulfur speciation	Fraction of captured sulfur as $S^{2-}/S^0/SO_4^{2-}$	XPS
Interfacial charge transfer	Change in metal-centre binding energy or Bader charge	XPS/XAS/DFT

Another important issue is the evaluation of adsorbents under real operating conditions [1]. Most reported studies employ dilute H_2S streams with inert gases under constant temperature and humidity. These experiments provide useful information but do not fully represent practical gas purification processes. Industrial gas streams, including biogas, natural gas, coke oven gas, synthesis gas, and landfill gas, typically contain CO_2, H_2O, O_2, NH_3, volatile organic compounds, siloxanes, and other sulfur-containing compounds. These components can compete for adsorption sites or alter sulfur transformation pathways [155]. In addition, changes in temperature, pressure, and operation mode further affect catalyst behavior. Under these conditions, active site evolution becomes more complex because adsorption, oxidation, reduction, and regeneration occur simultaneously at heterogeneous interfaces. Future studies should focus on long-term cyclic tests using multicomponent gas mixtures. Important factors include competitive adsorption, sulfur speciation, catalyst durability, and dynamic structural reconstruction in realistic conditions [44]. Connecting laboratory studies with industrial conditions is necessary to confirm the proposed mechanisms and identify practical limitations.

To transform the laboratory's success into industrially viable technology, future research must address the significant economic and scalability gap between MOFs and commercial benchmark products. Reported research-grade catalogue prices for selected MOFs (880–2200 US dollars per kilogram) are higher than the corresponding prices reported for activated carbon (93 US dollars per kilogram) and solid amine adsorbers (484 US dollars per kilogram) [156,157]. These values are not production costs and should not be generalized across materials or production scales. Although the following assessment was conducted for gas-storage MOFs rather than H_2S removal, a process-based techno-economic analysis of four representative MOFs at a 2.5 Mkg per year scale projects only 35–71 US dollars per kilogram for baseline solvothermal synthesis and 13–36 US dollars per kilogram for liquid-assisted-grinding or aqueous routes, with below 10 US dollars per kilogram identified as attainable [158]. Large-scale production nevertheless remains constrained by the challenges of continuous high-yield synthesis and binder-assisted molding technologies [156,157]. Future research should not compete with low-cost conventional commercial adsorbents, but should strategically target high-value application areas, such as biogas purification and electronic gas purification, where the higher selectivity of MOFs may justify their higher costs. At the same time, developing carbon materials derived from MOFs (estimated at 10–30 US dollars per kilogram; this figure remains a rough estimate pending dedicated techno-economic assessment) is a practical path to bridge the performance and cost gap. Overcoming these two obstacles through innovative low-cost synthesis and precise market positioning will be the key to realizing the potential of MOF-based hydrogen sulfide removal technology in industry.

Future research should combine real-time characterization with density functional theory, molecular dynamics, kinetic simulations, and machine-learning-assisted data analysis. These methods can help establish relationships linking atomic-scale evolution, intermediate formation, sulfur transport, and macroscopic adsorption performance [155]. Such integrated strategies can support catalyst design by considering the whole evolution process of active sites instead of only comparing the material before and after reaction.

Future MOF-based H_2S-removal materials should increasingly be viewed as dynamic porous systems in which adsorption sites and reactive interfaces can evolve under operating conditions. The ability to control structural reconstruction, interfacial electron transfer, sulfur migration, and regeneration behavior will determine whether high initial activity can be maintained during long-term operation. Achieving this objective requires cooperation among materials chemistry, catalysis, spectroscopy, computational science, artificial intelligence, and

process engineering. By integrating these complementary disciplines, dynamic active site engineering is expected to evolve from a mechanistic concept into a practical design strategy for highly regenerable adsorbents operating under realistic gas purification conditions. These developments can improve H_2S removal technologies and provide new ideas for designing adaptive porous catalysts for sustainable environmental and energy applications.

Ultimately, in order to advance the MOF-based H_2S adsorbents from the proof-of-concept stage to practical application, a standardized cyclic evaluation protocol is urgently needed in this field. We propose a benchmark of at least 5 consecutive adsorption-regeneration cycles with regeneration conditions reported explicitly. This threshold is set at the level already achieved by the best-documented studies here rather than imposed arbitrarily (only 3 of 17 entries in Table 5 report ≥ 5 cycles; longer tests are preferable where feasible). A common baseline of this kind would make retention data comparable across studies and support more reliable assessment of long-term behavior.

8. Conclusions

MOF-based adsorbents have created new opportunities for H_2S removal by controlling pore structures, metal coordination environments, and interfacial functionalities. However, most previous studies have focused on initial adsorption capacity and breakthrough performance. The changes of active sites during sulfur adsorption and regeneration are still not fully understood. This review shows that H_2S removal is not a simple adsorption process. It involves several continuous steps, including molecular adsorption, surface activation, sulfur transformation, interface reconstruction, and active site recovery.

The development of pristine MOFs to functionalized, derived, and hybrid materials shows the importance of synergistic regulation of metal sites, functional groups, pore structures, and interfaces. Future material designs should prioritize not only increasing adsorption sites but also enhancing active site adaptability and regeneration stability.

During H_2S removal, metal species, nitrogen functionalities, and sulfur intermediates undergo state-dependent electronic and structural changes, which can influence adsorption efficiency and regeneration behavior. Therefore, active sites in MOF-based adsorbents should be regarded as dynamic entities rather than fixed adsorption centers. Regeneration strategies, including thermal and chemical approaches, should be integrated into material design by considering sulfur migration, metal-sulfur interaction, and interfacial reconstruction.

Future studies should focus on establishing relationships between dynamic structural changes and overall performance. The combination of operando characterization, multiscale simulations, and AI-guided materials design may help develop MOF structures with better adsorption and regeneration performance. At the same time, practical applications require further testing under real gas mixtures, long-term operation, and scalable preparation conditions.

Overall, dynamic active site engineering provides a new way to understand and design regenerable MOF-based H_2S adsorbents. Controlling molecular interaction and regulating interface changes can help future materials move beyond high initial adsorption capacity toward stable, energy-saving, and practical sulfur purification technologies.

Author Contributions

R.Q.: conceptualization, methodology, literature investigation, data curation, visualization, original draft preparation, review and editing; X.N.: literature investigation, data curation, visualization; Y.Y.: literature investigation, review and editing; S.J.: literature investigation, review and editing; Q.X.: conceptualization, supervision, project administration, review and editing. All authors have read and agreed to the published version of the manuscript.

Funding

This research was funded by Qiyong Xu grant number 22576006 and 42307476 in this section.

Institutional Review Board Statement

Not applicable, as this study did not involve humans or animals.

Informed Consent Statement

Not applicable, as this study did not involve humans or subjects.

Data Availability Statement

No new data were generated or analyzed in this study. All information discussed in this review was obtained from previously published literature and is appropriately cited in the manuscript.

Acknowledgments

The authors greatly appreciate the financial support by the National Natural Science Foundation of China (Grant Nos. 22576006 and 42307476).

Conflicts of Interest

The authors declare no conflict of interest.

Use of AI and AI-Assisted Technologies

During the preparation of this work, the authors used ChatGPT (OpenAI) to assist with language polishing and improving the clarity of the manuscript. After using this tool, the authors reviewed and edited the content as needed and take full responsibility for the content of the published article.

References

1. Georgiadis, A.G.; Charisiou, N.; Yentekakis, I.V.; et al. Hydrogen sulfide (H2S) removal via MOFs. *Materials* **2020**, *13*, 3640. https://doi.org/10.3390/ma13163640.
2. De Crisci, A.G.; Moniri, A.; Xu, Y. Hydrogen from hydrogen sulfide: Towards a more sustainable hydrogen economy. *Int. J. Hydrogen Energy* **2019**, *44*, 1299–1327. https://doi.org/10.1016/j.ijhydene.2018.10.035.
3. Yentekakis, I.V.; Goula, G. Biogas management: Advanced utilization for production of renewable energy and added-value chemicals. *Front. Environ. Sci.* **2017**, *5*, 7. https://doi.org/10.3389/fenvs.2017.00007.
4. Charisiou, N.D.; Siakavelas, G.; Papageridis, K.N.; et al. Syngas production via the biogas dry reforming reaction over nickel supported on modified with CeO_2 and/or La_2O_3 alumina catalysts. *J. Nat. Gas Sci. Eng.* **2016**, *31*, 164–183. https://doi.org/10.1016/j.jngse.2016.02.021.
5. Huang, D.; Zhang, R.; Wang, N.; et al. Microbial assembly regulated microbial succession of biochar-mediated CH4 biofiltration to resume function under H_2S stress. *Chem. Eng. J.* **2025**, *506*, 160071. https://doi.org/10.1016/j.cej.2025.160071.
6. Huang, D.; Liang, M.; Wang, N.; et al. The efficiency and mechanism of humidity in alleviating CO_2 inhibition on H_2S adsorption to straw biochars. *Environ. Res.* **2022**, *210*, 113008. https://doi.org/10.1016/j.envres.2022.113008.
7. Yang, K.; Xu, Q.; Townsend, T.G.; et al. Hydrogen sulfide generation in simulated construction and demolition debris landfills: Impact of waste composition. *J. Air Waste Manag. Assoc.* **2006**, *56*, 1130–1138. https://doi.org/10.1080/10473289.2006.10464544.
8. Xu, Q.; Powell, J.; Jain, P.; et al. Modeling of H_2S migration through landfill cover materials. *J. Hazard. Mater.* **2014**, *264*, 254–260. https://doi.org/10.1016/j.jhazmat.2013.11.005.
9. Qi, R.; Yang, Y.; Sheng, K.; et al. Electrochemical removal of hydrogen sulfide and recovery of the deposited sulfur on the anode from wastewater. *J. Environ. Chem. Eng.* **2024**, *12*, 114426. https://doi.org/10.1016/j.jece.2024.114426.
10. Qi, R.; Zhang, X.; Wu, A.; et al. Controlling the thickness and composition of stainless steel surface oxide film for anodic sulfide removal. *J. Clean. Prod.* **2023**, *389*, 136076. https://doi.org/10.1016/j.jclepro.2023.136076.
11. Zhang, X.; Qi, R.; Wu, A.; et al. Effective anodic sulfide removal catalyzed by single nickel atoms on nitrogen-doped graphene with stainless steel substrate. *Chem. Eng. J.* **2022**, *427*, 130963. https://doi.org/10.1016/j.cej.2021.130963.
12. Hu, Z.; Li, L.; Cen, X.; et al. Integrated urban water management by coupling iron salt production and application with biogas upgrading. *Nat. Commun.* **2023**, *14*, 6405. https://doi.org/10.1038/s41467-023-42158-w.
13. Lee, S.; Xu, Q.; Booth, M.; et al. Reduced sulfur compounds in gas from construction and demolition debris landfills. *Waste Manag.* **2006**, *26*, 526–533. https://doi.org/10.1016/j.wasman.2005.10.010.
14. Vikrant, K.; Kim, K.H.; Deep, A. Photocatalytic mineralization of hydrogen sulfide as a dual-phase technique for hydrogen production and environmental remediation. *Appl. Catal. B Environ.* **2019**, *259*, 118025. https://doi.org/10.1016/j.apcatb.2019.118025.
15. El-Melih, A.M.; Al Shoaibi, A.; Gupta, A.K. Reformation of hydrogen sulfide to hydrogen in the presence of xylene. *Appl. Energy* **2017**, *203*, 403–411. https://doi.org/10.1016/j.apenergy.2017.06.064.
16. Xu, Q.; Townsend, T.; Bitton, G. Inhibition of hydrogen sulfide generation from disposed gypsum drywall using chemical inhibitors. *J. Hazard. Mater.* **2011**, *191*, 204–211. https://doi.org/10.1016/j.jhazmat.2011.04.063.
17. Gao, X.; Xiao, Z.; Wu, P.; et al. Recent research advances in adsorption removal of gaseous hydrogen sulfide by biochar. *Fuel* **2025**, *388*, 134390. https://doi.org/10.1016/j.fuel.2025.134390.
18. Cui, S.; Zhao, Y.; Liu, Y.; et al. Preparation of straw porous biochars by microwave-assisted KOH activation for removal of gaseous H_2S. *Energy Fuels* **2021**, *35*, 18592–18603. https://doi.org/10.1021/acs.energyfuels.1c02241.
19. Nicolae, S.A.; Szilágyi, P.Á.; Titirici, M.M. Soft templating production of porous carbon adsorbents for CO_2 and H_2S capture. *Carbon* **2020**, *169*, 193–204. https://doi.org/10.1016/j.carbon.2020.07.064.

20. Abatzoglou, N.; Boivin, S. A review of biogas purification processes. *Biofuels Bioprod. Bioref.* **2009**, *3*, 42–71. https://doi.org/10.1002/bbb.117.
21. Ryckebosch, E.; Drouillon, M.; Vervaeren, H. Techniques for transformation of biogas to biomethane. *Biomass Bioenergy* **2011**, *35*, 1633–1645. https://doi.org/10.1016/j.biombioe.2011.02.033.
22. Li, X.; Han, J.; Liu, Y.; et al. Summary of research progress on industrial flue gas desulfurization technology. *Sep. Purif. Technol.* **2022**, *281*, 119849. https://doi.org/10.1016/j.seppur.2021.119849.
23. Sikarwar, D.; Bashir, Y.; Sharma, N.; et al. Critical perspective on the elimination of emerging contaminants from industrial wastewater via microbial electrochemical technologies. *Clean-Soil Air Water* **2024**, *52*, 2300346. https://doi.org/10.1002/clen.202300346.
24. Jusoh, N.; Adibah Tengku Hassan, T.N.; Suhaimi, N.H.; et al. Hydrogen sulfide removal from biogas: An overview of technologies emphasizing membrane separation. *Sep. Purif. Technol.* **2025**, *373*, 133466. https://doi.org/10.1016/j.seppur.2025.133466.
25. Silva, A.F.R.; Ricci, B.C.; Koch, K.; et al. Dissolved hydrogen sulfide removal from anaerobic bioreactor permeate by modified direct contact membrane distillation. *Sep. Purif. Technol.* **2020**, *233*, 116036. https://doi.org/10.1016/j.seppur.2019.116036.
26. Peng, L.; Shi, M.; Zhang, X.; et al. Facilitated transport separation of CO_2 and H_2S by supported liquid membrane based on task-specific protic ionic liquids. *Green Chem. Eng.* **2022**, *3*, 259–266. https://doi.org/10.1016/j.gce.2021.12.005.
27. Qi, R.; Lin, T.; Sheng, K.; et al. Insight into the effective electrocatalytic sulfide removal from aqueous solutions using surface oxidized stainless-steel anode and its desulfurization mechanism. *Sci. Total Environ.* **2024**, *931*, 172570. https://doi.org/10.1016/j.scitotenv.2024.172570.
28. Yin, M.; Pillai, S.C.; Bolan, N.; et al. Low temperature selective catalytic oxidation of H_2S: Influencing factors, mechanisms and regeneration. *Chem. Eng. J.* **2024**, *479*, 147854. https://doi.org/10.1016/j.cej.2023.147854.
29. Georgiadis, A.G.; Charisiou, N.D.; Goula, M.A. Removal of hydrogen sulfide from various industrial gases: A review of the most promising adsorbing materials. *Catalysts* **2020**, *10*, 521. https://doi.org/10.3390/catal10050521.
30. Song, L.; Yuan, Y.; Wang, Y.; et al. Cu-MOF-derived Cu nanoparticles decorated porous N-doped biochar for low-temperature H_2S desulfurization. *Fuel* **2024**, *368*, 131682. https://doi.org/10.1016/j.fuel.2024.131682.
31. Bamdad, H.; Hawboldt, K.; MacQuarrie, S. A review on common adsorbents for acid gases removal: Focus on biochar. *Renew. Sustain. Energy Rev.* **2018**, *81*, 1705–1720. https://doi.org/10.1016/j.rser.2017.05.261.
32. Montes, D.; Tocuyo, E.; González, E.; et al. Reactive H_2S chemisorption on mesoporous silica molecular sieve-supported CuO or ZnO. *Microporous Mesoporous Mater.* **2013**, *168*, 111–120. https://doi.org/10.1016/j.micromeso.2012.09.018.
33. Abdullah, A.H.; Mat, R.; Somderam, S.; et al. Hydrogen sulfide adsorption by zinc oxide-impregnated zeolite (synthesized from Malaysian kaolin) for biogas desulfurization. *J. Ind. Eng. Chem.* **2018**, *65*, 334–342. https://doi.org/10.1016/j.jiec.2018.05.003.
34. Li, Y. Research progress of hydrogen sulfide adsorption based on MOFs. *ChemistrySelect* **2021**, *6*, 9960–9968. https://doi.org/10.1002/slct.202102950.
35. Gupta, N.K.; Kim, S.; Bae, J.; et al. Fabrication of $Cu(BDC)_{0.5}(BDC\text{-}NH_2)_{0.5}$ metal-organic framework for superior H_2S removal at room temperature. *Chem. Eng. J.* **2021**, *411*, 128536. https://doi.org/10.1016/j.cej.2021.128536.
36. Choleva, E.; Mitsopoulos, A.; Dimitropoulou, G.; et al. Adsorption of hydrogen sulfide on activated carbon materials derived from the solid fibrous digestate. *Materials* **2023**, *16*, 5119. https://doi.org/10.3390/ma16145119.
37. Li, J.R.; Kuppler, R.J.; Zhou, H.C. Selective gas adsorption and separation in metal-organic frameworks. *Chem. Soc. Rev.* **2009**, *38*, 1477–1504. https://doi.org/10.1039/b802426j.
38. Han, X.; Yang, S.; Schröder, M. Porous metal–organic frameworks as emerging sorbents for clean air. *Nat. Rev. Chem.* **2019**, *3*, 108–118. https://doi.org/10.1038/s41570-019-0073-7.
39. Chen, Y.; Lu, W.; Schröder, M.; et al. Analysis and Refinement of Host–Guest Interactions in Metal–Organic Frameworks. *Acc. Chem. Res.* **2023**, *56*, 2569–2581. https://doi.org/10.1021/acs.accounts.3c00243.
40. Song, Y.; Ma, S. Pore engineering in metal–organic frameworks and covalent organic frameworks: Strategies and applications. *Chem. Sci.* **2025**, *16*, 11740–11767. https://doi.org/10.1039/d5sc01635e.
41. Yang, L.; Zhang, P.; Cui, J.; et al. The Chemistry of Metal–Organic Frameworks for Multicomponent Gas Separation. *Angew. Chem.-Int. Ed.* **2024**, *63*, e202414503. https://doi.org/10.1002/anie.202414503.
42. Rieth, A.J.; Wright, A.M.; Dincă, M. Kinetic stability of metal–organic frameworks for corrosive and coordinating gas capture. *Nat. Rev. Mater.* **2019**, *4*, 708–725. https://doi.org/10.1038/s41578-019-0140-1.
43. Hoang, T.L.G.; Doan, D.T.; Nanda, S.; et al. Development of metal-organic framework-based systems for H_2S removal: A comprehensive review. *Coord. Chem. Rev.* **2025**, *529*, 216466. https://doi.org/10.1016/j.ccr.2025.216466.
44. Obeso, J.L.; Amaro, D.R.; Flores, C.V.; et al. Chemical transformations of highly toxic H_2S to promising clean energy in MOFs. *Coord. Chem. Rev.* **2023**, *485*, 215135. https://doi.org/10.1016/j.ccr.2023.215135.

45. Kökçam-Demir, Ü.; Goldman, A.; Esrafili, L.; et al. Coordinatively unsaturated metal sites (open metal sites) in metal-organic frameworks: Design and applications. *Chem. Soc. Rev.* **2020**, *49*, 2751–2798. https://doi.org/10.1039/c9cs00609e.
46. Martínez-Ahumada, E.; López-Olvera, A.; Jancik, V.; et al. MOF Materials for the Capture of Highly Toxic H_2S and SO_2. *Organometallics* **2020**, *39*, 883–915. https://doi.org/10.1021/acs.organomet.9b00735.
47. Li, X.; Rong, H.; Zhang, J.; et al. Modulating the local coordination environment of single-atom catalysts for enhanced catalytic performance. *Nano Res.* **2020**, *13*, 1842–1855. https://doi.org/10.1007/s12274-020-2755-3.
48. Chen, Y.Z.; Zhang, R.; Jiao, L.; et al. Metal–organic framework-derived porous materials for catalysis. *Coord. Chem. Rev.* **2018**, *362*, 1–23. https://doi.org/10.1016/j.ccr.2018.02.008.
49. Liu, B.; Shioyama, H.; Akita, T.; et al. Metal-organic framework as a template for porous carbon synthesis. *J. Am. Chem. Soc.* **2008**, *130*, 5390–5391. https://doi.org/10.1021/ja7106146.
50. De Villenoisy, T.; Zheng, X.; Wong, V.; et al. Principles of design and synthesis of metal derivatives from MOFs. *Adv. Mater.* **2023**, *35*, 2210166. https://doi.org/10.1002/adma.202210166.
51. Huang, Y.; Yuan, Y.; Song, L.; et al. Magnesium-organic framework-derived MgO-supported nitrogen-doped biochar for ultrahigh-performance low-temperature H_2S desulfurization. *Sep. Purif. Technol.* **2025**, *368*, 133027. https://doi.org/10.1016/j.seppur.2025.133027.
52. Maiti, B.K.; Maia, L.B.; Moura, J.J.G. Sulfide and transition metals—A partnership for life. *J. Inorg. Biochem.* **2022**, *227*, 111687. https://doi.org/10.1016/j.jinorgbio.2021.111687.
53. Yang, Y.; Liu, X.; Yang, C.; et al. Study on the essential features for MOFs to reversible adsorption of H_2S at room temperature. *Colloids Surf. A Physicochem. Eng. Asp.* **2023**, *674*, 131914.
54. Wang, Y.; Duan, M.; Su, Z.; et al. Combination of adsorption and oxidation over Fe-doped Cu-1,3,5-benzenetricarboxylate to boost room temperature H2S removal. *Sep. Purif. Technol.* **2025**, *360*, 131044. https://doi.org/10.1016/j.seppur.2024.131044.
55. Chavan, S.; Bonino, F.; Valenzano, L.; et al. Fundamental Aspects of H_2S Adsorption on CPO-27-Ni. *J. Phys. Chem. C* **2013**, *117*, 15615–15622. https://doi.org/10.1021/jp402440u.
56. Allan, P.K.; Wheatley, P.S.; Aldous, D.; et al. Metal–organic frameworks for the storage and delivery of biologically active hydrogen sulfide. *Dalton Trans.* **2012**, *41*, 4060–4066. https://doi.org/10.1039/c2dt12069k.
57. Liu, J.; Wei, Y.; Li, P.; et al. Selective H_2S/CO_2 Separation by Metal–Organic Frameworks Based on Chemical-Physical Adsorption. *J. Phys. Chem. C* **2017**, *121*, 13249–13255. https://doi.org/10.1021/acs.jpcc.7b04465.
58. Furukawa, H.; Cordova, K.E.; O'Keeffe, M.; et al. The chemistry and applications of metal-organic frameworks. *Science* **2013**, *341*, 1230444. https://doi.org/10.1126/science.1230444.
59. Vaesen, S.; Guillerm, V.; Yang, Q.; et al. A robust amino-functionalized titanium(iv) based MOF for improved separation of acid gases. *Chem. Commun.* **2013**, *49*, 10082–10084. https://doi.org/10.1039/c3cc45828h.
60. Gupta, N.K.; Kim, S.; Bae, J.; et al. Chemisorption of hydrogen sulfide over copper-based metal–organic frameworks: Methanol and UV-assisted regeneration. *RSC Adv.* **2021**, *11*, 4890–4900. https://doi.org/10.1039/d0ra09017d.
61. Ethiraj, J.; Bonino, F.; Lamberti, C.; et al. H_2S interaction with HKUST-1 and ZIF-8 MOFs: A multitechnique study. *Microporous Mesoporous Mater.* **2015**, *207*, 90–94. https://doi.org/10.1016/j.micromeso.2014.12.034.
62. Lee, M.H.; Vikrant, K.; Younis, S.A.; et al. Chemisorption of hydrogen sulfide by metal-organic frameworks and covalent-organic polymers based on experimental/theoretical evaluation. *J. Clean. Prod.* **2020**, *250*, 119486. https://doi.org/10.1016/j.jclepro.2019.119486.
63. Li, Z.; Liao, F.; Jiang, F.; et al. Capture of H_2S and SO_2 from trace sulfur containing gas mixture by functionalized UiO-66(Zr) materials: A molecular simulation study. *Fluid Phase Equilib.* **2016**, *427*, 259–267. https://doi.org/10.1016/j.fluid.2016.07.020.
64. Sokhanvaran, V.; Gomar, M.; Yeganegi, S. H_2S separation from biogas by adsorption on functionalized MIL-47-X (X = −OH and $-OCH_3$): A simulation study. *Appl. Surf. Sci.* **2019**, *479*, 1006–1013. https://doi.org/10.1016/j.apsusc.2019.02.152.
65. Hamon, L.; Leclerc, H.; Ghoufi, A.; et al. Molecular Insight into the Adsorption of H_2S in the Flexible MIL-53(Cr) and Rigid MIL-47(V) MOFs: Infrared Spectroscopy Combined to Molecular Simulations. *J. Phys. Chem. C* **2011**, *115*, 2047–2056. https://doi.org/10.1021/jp1092724.
66. Zárate, J.A.; Sánchez-González, E.; Jurado-Vázquez, T.; et al. Outstanding reversible H_2S capture by an Al(III)-based MOF. *Chem. Commun.* **2019**, *55*, 3049–3052. https://doi.org/10.1039/c8cc09379b.
67. Pourreza, A.; Askari, S.; Rashidi, A.; et al. Highly efficient SO_3Ag-functionalized MIL-101(Cr) for adsorptive desulfurization of the gas stream: Experimental and DFT study. *Chem. Eng. J.* **2019**, *363*, 73–83. https://doi.org/10.1016/j.cej.2019.01.133.
68. Xu, J.; Xing, W.; Wang, H.; et al. Monte Carlo simulation study of the halogenated MIL-47(V) frameworks: Influence of functionalization on H_2S adsorption and separation properties. *J. Mater. Sci.* **2016**, *51*, 2307–2319. https://doi.org/10.1007/s10853-015-9539-2.

69. Su, Y.M.; Huang, C.Y.; Chyou, Y.P.; et al. Sulfidation/regeneration multi-cyclic testing of Fe_2O_3/Al_2O_3 sorbents for the high-temperature removal of hydrogen sulfide. *J. Taiwan Inst. Chem. Eng.* **2017**, *74*, 89–95. https://doi.org/10.1016/j.jtice.2016.12.011.
70. Shi, L.; Yang, K.; Zhao, Q.; et al. Characterization and Mechanisms of H_2S and SO_2 Adsorption by Activated Carbon. *Energy Fuels* **2015**, *29*, 6678–6685. https://doi.org/10.1021/acs.energyfuels.5b01696.
71. Zhang, J.; Song, H.; Chen, Y.; et al. Amino-modified molecular sieves for adsorptive removal of H_2S from natural gas. *RSC Adv.* **2018**, *8*, 38124–38130. https://doi.org/10.1039/c8ra06859c.
72. Rezaei, S.; Tavana, A.; Sawada, J.A.; et al. Novel Copper-Exchanged Titanosilicate Adsorbent for Low Temperature H_2S Removal. *Ind. Eng. Chem. Res.* **2012**, *51*, 12430–12434. https://doi.org/10.1021/ie300244y.
73. Khalili, A.A.; Yeganegi, S. Computational study of the effect of functionalization on natural gas components separation and adsorption in NUM-3a MOF. *J. Mol. Graph. Model.* **2020**, *101*, 107731. https://doi.org/10.1016/j.jmgm.2020.107731.
74. Díaz-Ramírez, M.L.; Sánchez-González, E.; Álvarez, J.R.; et al. Partially fluorinated MIL-101(Cr): From a miniscule structure modification to a huge chemical environment transformation inspected by ^{129}Xe NMR. *J. Mater. Chem. A* **2019**, *7*, 15101–15112. https://doi.org/10.1039/c9ta02237f.
75. Hamon, L.; Serre, C.; Devic, T.; et al. Comparative study of hydrogen sulfide adsorption in the MIL-53(Al, Cr, Fe), MIL-47(V), MIL-100(Cr), and MIL-101(Cr) metal−organic frameworks at room temperature. *J. Am. Chem. Soc.* **2009**, *131*, 8775–8777. https://doi.org/10.1021/ja901587t.
76. Shahsavani, A.; Ahadi, Z.; Sokhanvaran, V.; et al. Dynamics and separation-based adsorption of binary mixtures of CH_4, CO_2 and H_2S on MIL-47: GCMC and MD studies. *J. Nanoanalysis* **2019**, *6*, 48–59.
77. Petit, C.; Levasseur, B.; Mendoza, B.; et al. Reactive adsorption of acidic gases on MOF/graphite oxide composites. *Microporous Mesoporous Mater.* **2012**, *154*, 107–112. https://doi.org/10.1016/j.micromeso.2011.09.012.
78. Petit, C.; Mendoza, B.; Bandosz, T.J. Hydrogen sulfide adsorption on MOFs and MOF/graphite oxide composites. *ChemPhysChem* **2010**, *11*, 3678–3684. https://doi.org/10.1002/cphc.201000689.
79. Zheng, F.; Xia, G.; Yang, Y.; et al. MOF-derived ultrafine MnO nanocrystals embedded in a porous carbon matrix as high-performance anodes for lithium-ion batteries. *Nanoscale* **2015**, *7*, 9637–9645. https://doi.org/10.1039/c5nr00528k.
80. Wang, Z.; Yan, T.; Shi, L.; et al. *In situ* expanding pores of dodecahedron-like carbon frameworks derived from MOFs for enhanced capacitive deionization. *ACS Appl. Mater. Interfaces* **2017**, *9*, 15068–15078. https://doi.org/10.1021/acsami.7b02712.
81. Gao, T.; Liu, Z.; Li, H. Heteroatom doping modified hierarchical mesoporous carbon derived from ZIF-8 for capacitive deionization with enhanced salt removal rate. *Sep. Purif. Technol.* **2020**, *231*, 115918. https://doi.org/10.1016/j.seppur.2019.115918.
82. Chen, J.; Jing, Y.; Song, X.; et al. Dual MOF-derived porous carbon composites: Preparation of efficient bifunctional catalysts by pyrolytic protection strategy. *J. Solid State Chem.* **2026**, *356*, 125810. https://doi.org/10.1016/j.jssc.2026.125810.
83. Liang, Z.; Zhao, R.; Qiu, T.; et al. Metal-organic framework-derived materials for electrochemical energy applications. *EnergyChem* **2019**, *1*, 100001. https://doi.org/10.1016/j.enchem.2019.100001.
84. Huang, Y.; Chen, Y.; Xu, M.; et al. Catalysts by pyrolysis: Transforming metal-organic frameworks (MOFs) precursors into metal-nitrogen-carbon (M-N-C) materials. *Mater. Today* **2023**, *69*, 66–78. https://doi.org/10.1016/j.mattod.2023.08.007.
85. Hernández-Ferrer, J.; Gracia-Martín, M.; Benito, A.M.; et al. Effect of temperature and presence of minor amount of metal on porous carbon materials derived from ZIF8 pyrolysis for electrocatalysis. *Catal. Today* **2023**, *423*, 113993. https://doi.org/10.1016/j.cattod.2022.12.024.
86. Xu, Q.; Guo, Z.; Zhang, M.; et al. Highly efficient photocatalysts by pyrolyzing a Zn–Ti heterometallic metal–organic framework. *CrystEngComm* **2016**, *18*, 4046–4052. https://doi.org/10.1039/c5ce01439e.
87. Jiang, H.L.; Liu, B.; Lan, Y.Q.; et al. From Metal–Organic Framework to Nanoporous Carbon: Toward a Very High Surface Area and Hydrogen Uptake. *J. Am. Chem. Soc.* **2011**, *133*, 11854–11857. https://doi.org/10.1021/ja203184k.
88. Shan, L.; Liu, X.; Zhao, Y.; et al. Hierarchical porous N-doped carbon particles derived from ZIF-8 as highly efficient H2S selective oxidation catalysts. *ACS Appl. Mater. Interfaces* **2024**, *16*, 23314–23324. https://doi.org/10.1021/acsami.4c02236.
89. Zhou, Q.; Yan, S.; Zhang, L. Fe-doped MOF-derived N-rich porous carbon nanoframe for H_2S cataluminescence sensing. *Luminescence* **2022**, *37*, 1135–1144. https://doi.org/10.1002/bio.4267.
90. Pokhrel, J.; Bhoria, N.; Wu, C.; et al. Cu- and Zr-based metal organic frameworks and their composites with graphene oxide for capture of acid gases at ambient temperature. *J. Solid State Chem.* **2018**, *266*, 233–243. https://doi.org/10.1016/j.jssc.2018.07.022.
91. Kim, D.; Kim, D.W.; Hong, W.G.; et al. Graphene/ZIF-8 composites with tunable hierarchical porosity and electrical conductivity. *J. Mater. Chem. A* **2016**, *4*, 7710–7717. https://doi.org/10.1039/c6ta01899h.
92. Chronopoulos, D.D.; Saini, H.; Tantis, I.; et al. Carbon Nanotube Based Metal–Organic Framework Hybrids from Fundamentals Toward Applications (Small 4/2022). *Small* **2022**, *18*, 2270017. https://doi.org/10.1002/smll.202270017.
93. Daraee, M.; Ghasemy, E.; Rashidi, A. Synthesis of novel and engineered UiO-66/graphene oxide nanocomposite with enhanced H_2S adsorption capacity. *J. Environ. Chem. Eng.* **2020**, *8*, 104351. https://doi.org/10.1016/j.jece.2020.104351.

94. Li, Y.; Yang, C.; Fan, H.; et al. Enhanced sulfur selectivity for H_2S catalytic oxidation over Fe_2O_3@UiO-66 catalyst. *Sep. Purif. Technol.* **2022**, *289*, 120791. https://doi.org/10.1016/j.seppur.2022.120791.
95. Daraee, M.; Saeedirad, R.; Rashidi, A. Adsorption of hydrogen sulfide over a novel metal organic framework–metal oxide nanocomposite: TOUO-x (TiO_2/UiO-66). *J. Solid State Chem.* **2019**, *278*, 120866. https://doi.org/10.1016/j.jssc.2019.07.027.
96. Ezugwu, C.I.; Christensen, F.M.S.; Xiong, X.; et al. Tuning adsorption selectivity of H_2S and CO_2 with robust bimetallic metal-organic frameworks. *Sep. Purif. Technol.* **2026**, *382*, 135996. https://doi.org/10.1016/j.seppur.2025.135996.
97. Zhang, H.Y.; Yang, C.; Geng, Q.; et al. Adsorption of hydrogen sulfide by amine-functionalized metal organic framework (MOF-199): An experimental and simulation study. *Appl. Surf. Sci.* **2019**, *497*, 143815. https://doi.org/10.1016/j.apsusc.2019.143815.
98. Bhoria, N.; Basina, G.; Pokhrel, J.; et al. Functionalization effects on HKUST-1 and HKUST-1/graphene oxide hybrid adsorbents for hydrogen sulfide removal. *J. Hazard. Mater.* **2020**, *394*, 122565. https://doi.org/10.1016/j.jhazmat.2020.122565.
99. Li, M.; Tang, M.; Xue, P.; et al. A binder-free, well-integrated metal–organic frameworks@polypyrrole nanofilm electrocatalyst for highly efficient and selective reduction of carbon dioxide. *Mater. Today Energy* **2022**, *30*, 101140. https://doi.org/10.1016/j.mtener.2022.101140.
100. He, X. Fundamental Perspectives on the Electrochemical Water Applications of Metal–Organic Frameworks. *Nano-Micro Lett.* **2023**, *15*, 148. https://doi.org/10.1007/s40820-023-01124-3.
101. Li, J.; Musho, T.; Bright, J.; et al. Functionalization of a metal-organic framework semiconductor for tuned band structure and catalytic activity. *J. Electrochem. Soc.* **2019**, *166*, H3029–H3034. https://doi.org/10.1149/2.0051905jes.
102. Wang, Y.; Yang, C.; Zhang, C.; et al. Effect of hierarchical porous MOF-199 regulated by PVP on their ambient desulfurization performance. *Fuel* **2022**, *319*, 123845. https://doi.org/10.1016/j.fuel.2022.123845.
103. Sun, M.; Wang, X.; Pan, X.; et al. Nitrogen-rich hierarchical porous carbon nanofibers for selective oxidation of hydrogen sulfide. *Fuel Process. Technol.* **2019**, *191*, 121–128. https://doi.org/10.1016/j.fuproc.2019.03.020.
104. Jia, N.; Fu, P.; Yang, J.; et al. Synergistic chemi-physisorption in NH_2-MIL-125/graphene aerogel composites for efficient H_2S abatement in heritage conservation environments. *npj Herit. Sci.* **2025**, *13*, 609. https://doi.org/10.1038/s40494-025-02190-z.
105. Li, B.; Wen, H.M.; Zhou, W.; et al. Porous metal–organic frameworks for gas storage and separation: What, how, and why? *J. Phys. Chem. Lett.* **2014**, *5*, 3468–3479. https://doi.org/10.1021/jz501586e.
106. Marín-Rosas, P.; Hernández-Monsalvo, A.; Estrella-Gutiérrez, M.A.; et al. Detection and capture of highly toxic H_2S in porous cage-like materials: MOFs, COFs and POCs. *Inorg. Chem. Front.* **2026**, *13*, 5070–5088. https://doi.org/10.1039/d6qi00068a.
107. Zhang, G.; Liu, F.; Qu, Y.; et al. Controllable creating mesoporous coordination unsaturated sites in UiO-66 single crystals for efficient conversion of hydrogen sulfide into polysulphur. *Chem. Eng. J.* **2024**, *479*, 147565. https://doi.org/10.1016/j.cej.2023.147565.
108. Yu, Z.; Wang, X.; Hou, Y.N.; et al. Nitrogen-doped mesoporous carbon nanosheets derived from metal-organic frameworks in a molten salt medium for efficient desulfurization. *Carbon* **2017**, *117*, 376–382. https://doi.org/10.1016/j.carbon.2017.02.100.
109. Chen, S.; Liu, C.; Wang, J.; et al. Two-dimensional MOF-derived porous nanosheets dotted with *in-situ* MgO/carbon heterostructure achieving striking performance in H2S catalytic oxidation at room temperature. *Appl. Catal. B Environ. Energy* **2025**, *366*, 125005. https://doi.org/10.1016/j.apcatb.2024.125005.
110. Zhang, G.; Qu, Y.; Zhu, Q.; et al. Hierarchically porous UiO-66-Fe with coordinatively unsaturated bimetallic sites for high-efficiency selective oxidation of hydrogen sulfide. *Green Energy Environ.* **2026**, *in press*. https://doi.org/10.1016/j.gee.2026.03.007.
111. Zhang, H.Y.; Shi, R.H.; Fan, H.L.; et al. Defect creation by benzoic acid in Cu-based metal−organic frameworks for enhancing sulfur capture. *Microporous Mesoporous Mater.* **2020**, *298*, 110070. https://doi.org/10.1016/j.micromeso.2020.110070.
112. Wang, W.; Chen, L.; Riemenschneider, L.; et al. Highly Sensitive and Selective Zinc-Based Metal–Organic Framework Derivatives Gas Sensors for Trace H_2S Detection. *ACS Sens.* **2025**, *10*, 7584–7598. https://doi.org/10.1021/acssensors.5c01743.
113. Chen, Z.; Ling, L.; Wang, B.; et al. Adsorptive desulfurization with metal-organic frameworks: A density functional theory investigation. *Appl. Surf. Sci.* **2016**, *387*, 483–490. https://doi.org/10.1016/j.apsusc.2016.06.078.
114. Braga, M.U.C.; Perin, G.H.; de Oliveira, L.H.; et al. DFT calculations for adsorption of H_2S and other natural gas compounds on M-BTC MOF clusters. *Adsorption* **2024**, *30*, 519–535. https://doi.org/10.1007/s10450-024-00439-w.
115. Van de Voorde, B.; Hezinová, M.; Lannoeye, J.; et al. Adsorptive desulfurization with CPO-27/MOF-74: An experimental and computational investigation. *Phys. Chem. Chem. Phys.* **2015**, *17*, 10759–10766. https://doi.org/10.1039/c5cp01063b.
116. Wang, Y.; Duan, M.; Su, Z.; et al. Fe^{2+}-triggered unexpected room temperature H_2S catalytic oxidation activity in MIL-100(Fe). *Sep. Purif. Technol.* **2025**, *365*, 132695. https://doi.org/10.1016/j.seppur.2025.132695.

117. Feng, L.; Yuan, S.; Zhang, L.L.; et al. Creating Hierarchical Pores by Controlled Linker Thermolysis in Multivariate Metal–Organic Frameworks. *J. Am. Chem. Soc.* **2018**, *140*, 2363–2372. https://doi.org/10.1021/jacs.7b12916.
118. Gupta, N.K.; Kim, E.J.; Bae, J.; et al. Probing the origin and stability of bivalency in copper based porous coordination network and its application for H_2S gas capture. *Sci. Rep.* **2022**, *12*, 15388. https://doi.org/10.1038/s41598-022-19808-y.
119. Mandel, R.M.; Lotlikar, P.S.; Runčevski, T.; et al. Transdermal Hydrogen Sulfide Delivery Enabled by Open-Metal-Site Metal–Organic Frameworks. *J. Am. Chem. Soc.* **2024**, *146*, 18927–18937. https://doi.org/10.1021/jacs.4c00674.
120. Zheng, X.; Qi, S.; Cao, Y.; et al. Morphology evolution of acetic acid-modulated MIL-53(Fe) for efficient selective oxidation of H_2S. *Chin. J. Catal.* **2021**, *42*, 279–287. https://doi.org/10.1016/s1872-2067(20)63625-7.
121. Wang, Y.; Liu, X.; Duan, M.; et al. Synergistic effect of bimetal in isoreticular Zn–Cu–1,3,5-benzenetricarboxylate on room temperature gaseous sulfides removal. *J. Colloid Interface Sci.* **2023**, *641*, 707–718. https://doi.org/10.1016/j.jcis.2023.03.108.
122. Li, Z.; She, C.; Yao, Q.; et al. Screening of bimetallic TM-Cu-BTCs for H_2S gas sensor materials and sensing mechanism study: A DFT study. *Mater. Today Chem.* **2025**, *48*, 102969. https://doi.org/10.1016/j.mtchem.2025.102969.
123. Sun, M.; Wang, X.; Li, Y.; et al. Selective catalytic oxidation of pollutant H_2S over Co-decorated hollow N-doped carbon nanofibers for high-performance Li-S batteries. *Appl. Catal. B Environ.* **2022**, *317*, 121763. https://doi.org/10.1016/j.apcatb.2022.121763.
124. Chen, L.; Jiang, X.; Ma, S.; et al. Towards highly exposed active sites via edge-N-rich carbon nanosheet@porous biochar for efficient H_2S catalytic oxidation. *Chem. Eng. J.* **2023**, *475*, 146115. https://doi.org/10.1016/j.cej.2023.146115.
125. Liu, X.; Fu, H.; Xu, C.; et al. Stable and active axial N-coordinated Ni single-atom catalyst for catalytic desulfurization. *ACS Catal.* **2026**, *16*, 4690–4700. https://doi.org/10.1021/acscatal.5c08112.
126. Wen, Z.; Jia, D.; Shen, Z.; et al. MOFs-derived nitrogen-doped hierarchically porous carbon for high-performance zinc-iodine batteries. *Clean Coal Technol.* **2025**, *31*, 243–252.
127. Zheng, Y.; Cheng, P.; Xu, J.; et al. MOF-derived nitrogen-doped nanoporous carbon for electroreduction of CO_2 to CO: The calcining temperature effect and the mechanism. *Nanoscale* **2019**, *11*, 4911–4917. https://doi.org/10.1039/c8nr10236h.
128. Gupta, N.K.; Bae, J.; Kim, S.; et al. Fabrication of Zn-MOF/ZnO nanocomposites for room temperature H_2S removal: Adsorption, regeneration, and mechanism. *Chemosphere* **2021**, *274*, 129789. https://doi.org/10.1016/j.chemosphere.2021.129789.
129. Gupta, N.K.; Bae, J.; Kim, K.S. From MOF-199 Microrods to CuO Nanoparticles for Room-Temperature Desulfurization: Regeneration and Repurposing Spent Adsorbents as Sustainable Approaches. *ACS Omega* **2021**, *6*, 25631–25641. https://doi.org/10.1021/acsomega.1c03712.
130. Zhang, H.Y.; Zhang, Z.R.; Yang, C.; et al. A computational study of the adsorptive removal of H_2S by MOF-199. *J. Inorg. Organomet. Polym. Mater.* **2018**, *28*, 694–701. https://doi.org/10.1007/s10904-017-0740-4.
131. Ru, Z.; Zhang, X.; Zhang, M.; et al. Bimetallic-MOF-Derived $Zn_xCo_{3-x}O_4$/Carbon Nanofiber Composited Sorbents for High-Temperature Coal Gas Desulfurization. *Environ. Sci. Technol.* **2022**, *56*, 17288–17297. https://doi.org/10.1021/acs.est.2c04193.
132. Liu, Y.; Song, C.; Wang, Y.; et al. Rational designed Co@N-doped carbon catalyst for high-efficient H2S selective oxidation by regulating electronic structures. *Chem. Eng. J.* **2020**, *401*, 126038. https://doi.org/10.1016/j.cej.2020.126038.
133. Gu, J.; Chen, Y.; Chen, G. Overcoming the "trade-off" issue: Multiscale computational screening of promising MOFs with rich oxygen sites on H_2S/CH_4 separation. *Fuel* **2025**, *402*, 136004. https://doi.org/10.1016/j.fuel.2025.136004.
134. Grubišić, S.; Dahmani, R.; Djordjević, I.; et al. Selective adsorption of sulphur dioxide and hydrogen sulphide by metal–organic frameworks. *Phys. Chem. Chem. Phys.* **2023**, *25*, 954–965. https://doi.org/10.1039/d2cp04295a.
135. Tavakol, H.; Haghshenas, H. A DFT study on the interaction of doped carbon nanotubes with H_2S, SO_2 and thiophene. *Quantum Rep.* **2021**, *3*, 366–375. https://doi.org/10.3390/quantum3030023.
136. Zheng, X.; Zhang, L.; Fan, Z.; et al. Enhanced catalytic activity over MIL-100(Fe) with coordinatively unsaturated Fe^{2+}/Fe^{3+} sites for selective oxidation of H_2S to sulfur. *Chem. Eng. J.* **2019**, *374*, 793–801. https://doi.org/10.1016/j.cej.2019.05.228.
137. Fujisaki, T.; Ikeda, K.; Staykov, A.; et al. Density functional theory analysis for H_2S adsorption on pyridinic N- and oxidized N-doped graphenes. *RSC Adv.* **2022**, *12*, 19955–19964. https://doi.org/10.1039/d2ra00898j.
138. Liu, X.; Shan, L.; Sun, X.; et al. Reusable salt-template strategy for synthesis of porous nitrogen-rich carbon boosts H_2S selective oxidation. *Green Energy Environ.* **2024**, *9*, 1866–1877. https://doi.org/10.1016/j.gee.2024.01.005.
139. Xing, X.; Zhang, X.; Tang, J.; et al. Selective catalytic oxidation of H_2S over Fe_2O_3/TiO_2 catalysts. *J. China Coal Soc.* **2021**, *46*, 1088–1095.
140. Zhang, Q.; Zheng, C.; Zhang, K.; et al. Ce–Mn Oxide Nanocomposites for Catalytic Removal of H_2S. *ACS Appl. Nano Mater.* **2023**, *6*, 2585–2595. https://doi.org/10.1021/acsanm.2c04959.
141. Zhang, D.; Sun, Y.; Wen, H.; et al. Preparation and H2S removal properties of ACF adsorbent supported by MOFs. *Fine Chem.* **2024**, *41*, 1710–1717.

142. Huang, D.; Wang, N.; Bai, X.; et al. The influencing mechanism of O_2, H_2O, and CO_2 on the H_2S removal of food waste digestate-derived biochar with abundant minerals. *Biochar* **2022**, *4*, 71. https://doi.org/10.1007/s42773-022-00199-2.
143. Paz, L.; Gentil, S.; Fierro, V.; et al. Activated carbons outperform other sorbents for biogas desulfurization. *Chem. Eng. J.* **2025**, *506*, 160304. https://doi.org/10.1016/j.cej.2025.160304.
144. Al-Janabi, N.; Hill, P.; Torrente-Murciano, L.; et al. Mapping the Cu-BTC metal–organic framework (HKUST-1) stability envelope in the presence of water vapour for CO_2 adsorption from flue gases. *Chem. Eng. J.* **2015**, *281*, 669–677. https://doi.org/10.1016/j.cej.2015.07.020.
145. Acuna-Yeomans, E.; Goosen, P.J.; Gutiérrez-Sevillano, J.J.; et al. Effect of water loading on the stability of pristine and defective UiO-66. *J. Mater. Chem. A* **2024**, *12*, 25233–25243. https://doi.org/10.1039/d4ta04252b.
146. Li, Y.; Liu, J.; Liu, F.; et al. Interaction mechanism between CO and H_2S over $CuFe_2O_4$ oxygen carrier during chemical-looping combustion: A DFT study. *Fuel* **2022**, *324*, 124720. https://doi.org/10.1016/j.fuel.2022.124720.
147. Gupta, N.K.; Vikrant, K.; Kim, K.S.; et al. Regeneration strategies for metal–organic frameworks post acidic gas capture. *Coord. Chem. Rev.* **2022**, *467*, 214629. https://doi.org/10.1016/j.ccr.2022.214629.
148. Kakaei, H.; Beygzadeh, M.; Golbabaei, F.; et al. Preparation of a sepiolite/Cu-BDC nanocomposite and its application as an adsorbent in respirator cartridges for H_2S removal. *New J. Chem.* **2019**, *43*, 11575–11584. https://doi.org/10.1039/c9nj01623f.
149. Wang, J.; Wang, L.; Fan, H.; et al. Highly porous copper oxide sorbent for H_2S capture at ambient temperature. *Fuel* **2017**, *209*, 329–338. https://doi.org/10.1016/j.fuel.2017.08.003.
150. Gupta, N.K.; Bae, J.; Kim, K.S. Bimetallic Ag–Cu-trimesate metal–organic framework for hydrogen sulfide removal. *New J. Chem.* **2021**, *45*, 22466–22477. https://doi.org/10.1039/d1nj04601b.
151. Li, X.; Zhang, X.; Zhang, J.; et al. Applied machine learning to analyze and predict CO_2 adsorption behavior of metal-organic frameworks. *Carbon Capture Sci. Technol.* **2023**, *9*, 100146. https://doi.org/10.1016/j.ccst.2023.100146.
152. Shayanmehr, M.; Aarabi, S.; Ghaemi, A.; et al. A data driven machine learning approach for predicting and optimizing sulfur compound adsorption on metal organic frameworks. *Sci. Rep.* **2025**, *15*, 3138. https://doi.org/10.1038/s41598-025-86689-2.
153. He, Y.; Han, R.; Wang, M.; et al. Machine learning-guided design of metal-organic frameworks for efficient H_2S/CH_4 separation. *J. Membr. Sci.* **2025**, *730*, 124207. https://doi.org/10.1016/j.memsci.2025.124207.
154. Ming, Z.; Qiao, Z.; Li, Z.; et al. Research advances in metal-organic frameworks with machine learning and big data mining. *J. Guangzhou Univ. Nat. Sci. Ed.* **2024**, *23*, 36–46.
155. Gao, W.; Zheng, W.; Yan, K.; et al. Accelerating the discovery of acid gas-selective MOFs for natural gas purification: A combination of machine learning and molecular fingerprint. *Fuel* **2023**, *350*, 128757. https://doi.org/10.1016/j.fuel.2023.128757.
156. Li, Z.; Yang, X.; Ju, C.; et al. Recent progress in the synthesis, scaling, processing and technoeconomic analysis of metal-organic frameworks towards industrial applications. *Mater. Sci. Eng. R Rep.* **2026**, *167*, 101123. https://doi.org/10.1016/j.mser.2025.101123.
157. Zhou, Z.; Yu, H.; Li, G.; et al. Material–scenario coupled techno-economics comparison of carbon capture adsorbents: Feasibility and suitability across various contexts. *Energy Convers. Manag.* **2026**, *348*, 120589. https://doi.org/10.1016/j.enconman.2025.120589.
158. DeSantis, D.; Mason, J.A.; James, B.D.; et al. Techno-economic analysis of metal–organic frameworks for hydrogen and natural gas storage. *Energy Fuels* **2017**, *31*, 2024–2032. https://doi.org/10.1021/acs.energyfuels.6b02510.